NAVORD REPORT 6683

(10)

MEASUREMENT OF THE CHARACTERISTICS OF THE COMPRESSIBLE TURBULENT BOUNDARY LAYER WITH AIR INJECTION (U)

3 SEPTEMBER 1959

U. S. NAVAL ORDNANCE LABORATORY
WHITE OAK, MARYLAND

U. S. NAVAL ORDNANCE LABORATORY

WHITE OAK
SILVER SPRING, MARYLAND

Change 1

To all holders of **NAVORD REPORT 6683**
insert change; write on cover 'Change inserted'
Approved by Commander, U.S. NOL pages

R. Kenneth Lobb
By direction

This publication is changed as follows:

1. **Please correct the author's name on the abstract cards, located in the back of NAVORD Report 6683, to read as**

   James E. Danberg

   in lieu of James E. Danbert.

Insert this change sheet between the cover and the title page of your copy.

NAVORD Report 6633

Aerodynamics Research Report No. 67

MEASUREMENT OF THE CHARACTERISTICS OF THE COMPRESSIBLE TURBULENT BOUNDARY LAYER WITH AIR INJECTION

Prepared by:

James E. Danberg

ABSTRACT: The compressible turbulent boundary layer on a porous flat plate with air injection has been studied experimentally in the Naval Ordnance Laboratory hypersonic wind tunnel. Boundary-layer velocity and temperature profiles were obtained at a Mach number of 5.1, a Reynolds number of 1.5×10^7 per meter, wall to free-stream temperature ratios of 4.2 and 5.0, and rates of air injection from zero to 0.08 percent of free-stream mass flow. Experimental values of skin friction were obtained from the velocity profiles and the results were compared with the theories of Rubesin and Persh. Neither theory predicts the experimental data on an absolute basis but Rubesin does describe the trend within ± 25 percent. The measured total temperature and velocity profiles compared favorably with the profiles assumed in Rubesin's theory. However, the Rubesin expression for the u^+ velocity at the interface between the laminar sublayer and the outer turbulent layer disagrees with experiment. The measurements indicate u^+ values of 14 ± 3, independent of both wall temperature and injection rate.

PUBLISHED JUNE 1960

U. S. NAVAL ORDNANCE LABORATORY
WHITE OAK, MARYLAND

This report presents the results of the first phase of a comprehensive program intended to extend the basic knowledge of the effect of mass transfer on hypersonic turbulent boundary layers. Knowledge concerning the characteristics of mass-transfer cooling has considerable current interest because of its potential applications in alleviating intense aerodynamic heating. Two of these applications are, first, the protection of missiles and space vehicles during atmosphere re-entry and, second, the protection of high performance rocket nozzles.

The next phase of this program will extend the range of the parameters studied, with particular attention to heat-transfer measurements, location of transition, and details of the profile near the sublayer.

This work was jointly sponsored by the U. S. Naval Bureau of Ordnance, the U. S. Air Force, the U. S. Army, and the Re-entry Body Section of the Special Projects Office, Bureau of Ordnance, under the Applied Research Program in Aeroballistics and Materials. It was carried out under Task Numbers NOL 502-335/51014/01, NOL 291, NOL 300, and NOL 363.

The author wishes to express his indebtedness to Mr. I. Korobkin and Dr. F. M. Winkler for many helpful discussions during the course of the investigations. The major part of the numerical evaluation was done by Mrs. Ada P. Jackson and Mr. M. H. Cha. Mr. Ralph Garren, Jr., in addition to participating in the tests, was largely responsible for the model design and test preparation.

MELL A. PETERSON
Captain, USN
Commander

R. KENNETH LOBB
By direction

CONTENTS

ILLUSTRATIONS

ILLUSTRATIONS

TABLES

SYMBOLS

C_f	skin-friction coefficient = $2\tau_w/\rho_\infty u_\infty^2$
C_q	nondimensional injection rate = $\rho_w v_w/\rho_\infty u_\infty$
K	constant = 0.4
1/n	exponent in the velocity profile
M	Mach number
p	pressure, mmHg
Pr	Prandtl number
Re	Reynolds number
r	recovery factor
T	Temperature, ^oK
u	velocity parallel to the surface, m/sec
u^+	nondimensional velocity = $u\sqrt{\rho_w/\tau_w}$
v	velocity of injected air normal to the surface, m/sec
y	distance normal to the surface, mm.
y^+	nondimensional distance from the wall= $y\sqrt{\tau_w\rho_w}/\mu_w$
δ	boundary-layer thickness, mm.
δ^*	boundary-layer displacement thickness, mm.
θ	boundary-layer momentum thickness, mm.
μ	coefficient of viscosity, Kg/m-sec
ρ	density, Kg/m^3
τ	shear stress, $Kg/m\text{-}sec^2$

SYMBOLS

Subscripts

a	an arbitrary point on the velocity profile in the turbulent outer layer
i	interface
m	measured or indicated
w	surface
x	distance from the leading edge
∞	free stream
e	adiabatic wall temperature
0	supply conditions
2	condition behind normal shock

INTRODUCTION

1. The high speed re-entry into the atmosphere of ballistic missiles and space vehicles requires the development of techniques for protecting their payload against the intense heating produced. One promising system is mass-transfer cooling. In fact, some nose cone materials ablate during re-entry and ablation under these conditions is a form of mass transfer cooling. For many years mass transfer techniques have been employed by turbo-jet and rocket engine manufacturers in protecting components exposed to high temperature combustion products. The missile application, however, differs from the engine application in the conditions outside the boundary layer.

2. Interest in this field has produced literature of considerable extent. Of particular interest are the incompressible turbulent boundary-layer measurements of Mickley, et al., (reference (a)) and the compressible laminar and turbulent boundary-layer measurements on porous cones and flat plates of Leadon and Scott (reference (b)) and Rubesin, Pappas, and Okuno (references (c) and (d)).

3. In order to increase the basic understanding and to extend the experimental data to higher speeds, the Naval Ordnance Laboratory has undertaken an extensive experimental program to study the hypersonic turbulent boundary layers with mass (gas) injection. The experiments reported herein represent only the first phase of this program and are a logical extension of the solid wall turbulent boundary-layer studies of reference (e).

4. This first phase of the program is concerned with measuring the pressure and temperature profiles on a porous flat plate at $M_\infty = 5.1$, a Reynolds number of 1.5×10^7 per meter, T_w/T_∞ of 4.2 and 5.0, and for rates of air injection from zero to 0.08 percent of the free-stream mass flow. From these profiles, values of skin-friction and other boundary-layer parameters were obtained.

Experimental Equipment and Techniques

5. The experiments described in this report have been conducted in the NOL Hypersonic Tunnel No. 4, the basic components of which are described in references (f) and (g). This wind tunnel is capable of operating continuously at Mach numbers from 5 to 10 with supply temperatures from 300°K to 800°K and supply pressures from 1 to 50 atmospheres. During

this particular experiment a Mach number 5.1 uniform-flow-nozzle was used with constant supply conditions of 380°K and 8 atmospheres.

6. The porous plate (Figure 1 and Figure 2) consisted of a flat plate (60.96x15.87 cm.) with a sharp leading edge (10° angle) and containing a sintered, woven, stainless-steel, wire-mesh insert (48.90x12.70x0.952 cm.). The porous material (manufactured by Aircraft Porous Media, Inc.) starts 6.98 cm. from the leading edge. The exposed side consisted of .127 mm. wire and was flat within a few tenths of a millimeter.

7. The porous material was tested for uniformity of mass flow with a venturi-tube flow meter. The calibration tests were performed at the correct operating pressures and temperatures on both sides of the porous material, thereby simulating the viscous and compressibility effects within the plate that are present during the actual wind-tunnel tests. The results showed the insert did not have the specified uniform mass-flow distribution. In two small regions near the center of the plate the mass flow/sq. cm. was twice the average while near the edges of the plate no flow was detected. The exact effect on the experiment of this non-uniformity is unknown now. However, the locations at which the boundary layer was investigated were more than 26 cm. down stream from the start of the porous insert and thus were influenced, to some extent, by about half the total injected mass.

8. The porous insert had 8 thermocouples cemented in the surface (Figure 1 and Figure 2). Six grooves 2.51 mm wide by .25 mm deep were machined in the exposed surface from the edge to the centerline of the plate and two others were placed diagonally so as to have at the 34.4 cm station three thermocouples, one on the centerline and two 1.27 and 3.31 cm from the centerline respectively. These provided a measurement of surface temperature and a check on its uniformity. The underside of the porous material was grooved and contained 15 U-shaped copper tubes. Silicon oil (Dow Corning DC-200, 2 centistoke) was circulated through these tubes entering at the downstream end of the plate passing up through the chamber beneath the plate and then back through the portion of each tube imbedded in the porous material. A view of the underside of the plate is shown in Figure 3. This system provided good temperature control and was necessary because the injected air was exposed to the hot back cover of the plate. The inside of the back cover forms the plenum chamber for the injected air. The temperature of the coolant and of the injected air was held constant by circulating them through separate copper coils immersed in a thermostatically controlled bath of either dry ice in alcohol or circulating tap water.

9. The boundary-layer measurements were made at two locations on the porous plate. One was 29.25 cm. and the other was 36.85 cm. from the leading edge. Previous results obtained with a solid flat plate (reference (e)) indicated that for the conditions of the present test, a fully developed turbulent boundary layer should exist at the two measuring stations.

10. At each station and for two essentially constant wall temperatures, namely, $T_w / T_\infty = 4.23$ and 5.04, the boundary layer was surveyed without injection and with four rates of air injection. The four injection rates are $\frac{\rho_w v_w}{\rho_\infty u_\infty} = 1.46\text{x}10^{-4}$ $4.24\text{x}10^{-4}$, $6.18\text{x}10^{-4}$, and $7.88\text{x}10^{-4}$. The injection rates are based on the total injected mass flowing through the porous insert as measured by a flowrater in the air supply line divided by the surface area of the plate. The injection rate is made dimensionless by dividing by the free-stream mass flow per unit area, $\rho_\infty u_\infty$.

11. Pitot pressure probes and total temperature probes were used to survey the boundary layer at both stations. In addition, static probe measurements were taken in the free-stream and for a short distance into the boundary layer. The Pitot probe and total temperature probe were essentially of the same external geometry. Both were made from thin-walled hypodermic tubing with a rectangular opening of half height .152 mm. The pressures were measured on either a mercury manometer with a range of 0 to 1 atmosphere absolute pressure or on a silicon oil manometer with a range of up to 35 mmHg. absolute. The reading accuracies of the two manometers were ± 0.1 mmHg. and ± 0.001 mmHg. respectively.

12. The internal construction of the total temperature probes was basically the same as the probes described in reference (f). In the present case, the probe consists of a .127 mm. iron-constantan thermocouple within a vented stainless-steel tube which serves as a radiation shield and as a device to establish known and constant flow conditions around the thermocouple junction. The latter is essential for obtaining a unique calibration in terms of $(T_m - T_\infty)/(T_o - T_\infty)$ as a function of the parameter $p_2/T_m^{7/4}$ (reference (f)). The probe was calibrated in the wind-tunnel free stream by varying the supply pressure and temperature so that the parameter $p_2/T_m^{7/4}$ was varied over the range encountered in the boundary-layer surveys. From this information, the local total temperature was

calculated from the indicated temperature, the local Mach number, and the Pitot pressure.

13. The above probes were supported in the tunnel by a traversing mechanism which allowed positioning of the probe with an accuracy of .025 mm. in a plane perpendicular to the centerline of the plate and extending from the plate surface about 7.62 cm. Each traverse was made from the free stream to the plate, the location of which was indicated by the completing of an electric circuit when the probe first touched the surface.

RESULTS

Boundary-Layer Profiles

14. The measured boundary-layer data are given in Tables 1 through 19. The Pitot pressures have been converted to Mach number by assuming constant static pressure through the boundary layer and using the standard flow tables for air, reference (i). The static temperature has been calculated from the probe indicated temperature with the use of the static pressure, local Mach number and by reference to the probe calibration curve. The velocity was calculated from this data using the standard flow equations.

15. Figures 4 through 11 contain the graphical representation of this tabulated data. The velocity distribution through the boundary layer (Figures 4 through 7) for zero blowing shows the typical, fully developed, turbulent profile. The air injection decreases the velocity more or less uniformly over a considerable part of the boundary layer and it also increases the total thickness. The distortion of the shape of the profile, due to the addition of air, occurs mostly at the point of greatest rate of change of curvature. At that point, the curves become flatter. The effect on the profile of changing the wall temperature and Reynolds number is difficult to detect with the limited data. There is evidence, however, that a decrease of the wall temperature produces the same sort of flattening near the knee of the curve as described above.

16. The general appearance of the total and static temperature distributions through the boundary layer (Figures 8 through 11), in the zero injection cases, is also that of fully developed turbulent profiles. Injection of air into the boundary layer decreases the total temperature in a manner

similar to the effect of injection on the velocity profile. The static temperature, however, increases with blowing rate.

Boundary-Layer Parameters

17. Certain properties of the boundary layer have been deduced from these profiles, such as: (Table 20)

δ, the total boundary-layer thickness
δ^*, the displacement thickness

$$\delta^* = \int_0^{\delta} \left(1 - \frac{\rho u}{\rho_\infty u_\infty}\right) dy \qquad (1)$$

θ, the momentum thickness

$$\theta = \int_0^{\delta} \frac{\rho u}{\rho_\infty u_\infty} \left(1 - \frac{u}{u_\infty}\right) dy \qquad (2)$$

where δ^* and θ were obtained from graphical integration of the profile data.

18. Each of these parameters increases roughly linearly with injection rate (Table 20). A decrease in wall temperature generally decreases slightly each thickness parameter, but the variation in wall temperature was too small for a quantitative statement.

19. The value of the ratio δ^*/θ, based upon these measurements, is between 10.5 and 11.5, independent of the injection rate.

20. n, the inverse of the velocity profile exponent in the equation

$$\frac{u}{u_\infty} = \left(\frac{y}{\delta}\right)^{1/n} \qquad (3)$$

was obtained from a log-log plot of the velocity against y. As might be expected, n decreases rapidly and nearly linearly with the injection rate. In fact, at $C_q \approx 8 \times 10^{-4}$, n has approximately one half of its zero injection value. The zero injection cases where n is $9 \pm .5$ are consistant with the impermeable wall data of reference (e), but are higher than the nozzle wall measurement of reference (j) ($5 \leq n \leq 7$).

Local Skin Friction

21. The skin friction was calculated in this experiment by extrapolating the velocity profile to the wall. There is an important difficulty in this procedure when there is blowing through the wall. That is, it is not necessary for the velocity to be zero at the wall. Since the wall is porous it is possible, on the average, for the injected air velocity to have a component along the plate. Since the shear stress can penetrate the pores, it is also possible that the velocity component has a preferred direction, that is down stream. Thus, whereas with an impermeable surface the velocity is interpolated, in the case of a porous surface it is an extrapolation. The present data do not necessarily indicate a zero velocity at the wall. Thus, the specific curve and the resulting skin-friction coefficient

$$C_f = 2\mu_w \left(\frac{\partial u}{\partial y_w}\right) / \rho_\infty u_\infty^2 \qquad (4)$$

depend strongly on the individual drawing the curve. Figures 12 through 15 show details of the last few measured points, i.e., in the region up to 1 mm from the wall. The skin-friction coefficients, C_f, have been calculated by the above formula and are based on a tentative extrapolation, as shown in Figures 12 through 15. If the velocity is forced to go through zero at y=0, the skin friction would be increased on the average by 44 percent, or in some cases, up to 100 percent.

22. As stated before, a fully developed turbulent boundary layer should be expected at about 21.6 cm. from the leading edge based on reference (e) results and from that point the local skin friction should monotonically decrease with increasing distance. The present results with $u_w \neq 0$ at the 29.25 cm. station do not show this decrease. With zero injection, the skin-friction coefficient is less than at the 36.85 cm. station. In fact, the C_f at 29.25 cm. is 30 percent lower than obtained under similar conditions on the solid flat plate. The present results might be interpreted as evidence of a later onset of transition or as a more extended transition region on the porous plate. On the other hand, if the velocity extrapolation is changed to give u=0 at the wall the corresponding C_f is increased. The 29.25 cm. station is then in better agreement with the previous solid flat-plate results but the 36.85 cm. station is considerably higher.

COMPARISON WITH THEORY

Skin Friction

23. Results in terms of C_f with $u_w \neq 0$ are shown in Figures 16 and 17, and included are the C_f calculations from the analytical approaches of Rubesin (reference (k)) and Persh (reference (l)). For the downstream station, the zero injection data are fairly closely predicted by both analyses. The upstream zero injection cases and all the blowing cases are as much as 50 percent below Rubesin's calculation. Persh's theory is also higher than the data for the upstream station but for C_q greater than 4.2×10^{-4}, the calculated values fall below the data. In order to demonstrate more clearly the trend of the experimental data with blowing rate, the results in terms of C_f to C_f without injection are plotted in Figure 18. The bands marked "theoretical curve" were obtained from references (k) and (l) by evaluating C_f for the Re_θ, n, T_w/T_∞ values associated with the experimental points. Each set of data exhibits a consistant decrease in C_f ratio with increasing C_q. Some of the data agree quite well with Rubesin's prediction.

Total Temperature Profiles

24. In addition to the direct comparison of skin-friction coefficient, the Crocco temperature-velocity relation as used in the analyses of references (k) and (l) has been checked against the experimental data. Usually, the Crocco equation is given in the form:

$$\frac{T}{T_\infty} = \frac{T_w}{T_\infty} + \left(\frac{T_e - T_w}{T_\infty}\right)\frac{u}{u_\infty} - \left(\frac{T_e - T_\infty}{T_\infty}\right)\left(\frac{u}{u_\infty}\right)^2 \qquad (5)$$

where

$$T_e = r\,(T_{o_\infty} - T_\infty) + T_\infty \qquad (6)$$

Both Rubesin and Persh, tentatively assume the recovery factor r invarient with injection rate. Rubesin used r=1 and Persh assumes $r = Pr^{1/3}$, where the Prandtl number (Pr) is evaluated at $T = T_w$. Using the experimental velocity distribution together with Equation (5) it was found that the experimental and computed temperature distributions generally agree within 5 to 8 percent. The momentum equation is, however, relatively insensitive to the temperature profile so that the computed temperature is probably acceptable in the analyses of references (k) and (l).

25. In order to obtain a more specific indication of the validity of the Crocco equation in describing the temperature-velocity relation in the turbulent boundary layer with air injection, a representation was chosen which tends to amplify the discrepancies. For this purpose Equation (5) was rewritten in the form

$$\frac{T_o - T_w}{T_{o_\infty} - T_w} = \frac{T_e - T_w}{T_{o_\infty} - T_w} \frac{u}{u} + \frac{T_{o_\infty} - T_e}{T_{o_\infty} - T_w} \left(\frac{u}{u_\infty}\right)^2 \qquad (7)$$

Figures 19 and 20 show the comparison of the experimental data with Equation (7), using r=1 and $r = Pr^{1/3}$. The computations were performed for selected values of the Mach number, wall and free-stream temperatures which are representative of the experimental test conditions, namely, an average Mach number M=5.08, T_w/T_∞ =4.23 and 5.05, and T_∞ =61.3°K. The four figures clearly show that the Crocco equation does not describe all details of the measured temperature-velocity distribution and its variation with heat transfer. The discrepancies are most pronounced for the conditions of largest heat transfer, T_w/T_∞ =4.23, Figures 19b and 20b. The deviations are up to 32 percent of $T_{o_\infty} - T_w$. In the outer turbulent portion $0.8 \leq u/u_\infty \leq 1$, the experimental data for each graph seem to define one curve, i.e., there is no noticeable effect due to the air injection. In addition, the data are fairly close to the Crocco prediction with $r = Pr^{1/3}$. When $u/u_\infty < 0.8$ the agreement with the theoretical curves is poor.

Velocity Profiles

26. The comparison of the experimental boundary-layer velocity profiles with the profiles assumed by Rubesin and Persh provides another check of the theories. As previously stated, neither of the theories accurately describes the experimentally determined variation of skin-friction coefficient with air injection (Figures 16 and 17). While Persh's theory predicts fairly accurately the value of the skin-friction coefficient for zero injection rate, it overestimates the effect of air injection. Rubesin's theory, on the other hand, predicts relatively closely the trend of changing skin-friction coefficient with air injection, but the absolute values of C_f are too high.

27. The Rubesin analysis describes the boundary-layer

velocity profile by two equations, one for the turbulent outer layer and one for the sublayer, and by an empirically determined interface which separates the two regions. The pertinent equations from reference (k) when modified for a finite velocity at the wall are:

Laminar sublayer $$\mu \frac{du}{dy} = \tau_w + \rho_w v_w (u-u_w) \qquad (8)$$

Turbulent outer layer $$\rho k^2 y^2 \left(\frac{du}{dy}\right)^2 = \tau_w + \rho_w v_w (u-u_w) \qquad (9)$$

Interface location $$u = u_i = 13.1 \sqrt{(\tau_w/\rho_w)(T_w/T_\infty)} \qquad (10)$$

28. Equation (10) was found inadequate for correctly predicting the location of the interface. Applying Equation (10) to the present experimental data, the calculated u_i was found, in most cases, to exceed the free-stream velocity. Therefore, it is useless in the present comparison for predicting the extent of the laminar sublayer.

29. In order to find a relation for u_i which more realistically describes the variation of the interface location and to determine how well Equations (8) and (9) describe the velocity profile with heat transfer and mass injection, the following procedure has been adopted. Equations (8) and (9) for the velocity profiles were numerically integrated using experimental values for skin friction, injection rates, and temperature profiles. The integration in the laminar sublayer was started at the wall where y=0 and $u=u_w$. In the turbulent case, the integration was started at a point on the experimental velocity profile judged to be well within the turbulent outer portion of the boundary layer. The intersection of the calculated profiles gives the interface velocity u_i.

30. The integration of Equation (8) results in the following:

$$\frac{u}{u_\infty} = \frac{u_w}{u_\infty} + \frac{C_f}{2C_q}\left[e^{\left(\frac{\rho_w v_w}{\mu_w}\int_0^y \frac{\mu_w}{\mu}\,dy\right)} - 1\right] \qquad (11)$$

where u can be obtained by numerically performing the integration and the lower limit of integration is y=0, $u=u_w$. There are two reasons why it is difficult to judge the adequacy of this equation to describe the profile. First, very few data points were measured within the region and second, the equation cannot predict the correct profile near the point of

intersection with the outer turbulent part since the region of transition from the laminar sublayer to the fully turbulent region (i.e., buffer layer) has been neglected. Nevertheless, the few points available which were assumed on the linear part of the velocity curve in determining the skin friction fall below the curve defined by the above equation.

31. Integration of Equation (9) gives

$$\frac{u}{u_\infty} = \frac{u_w}{u_\infty} + \frac{1}{C_q}\left\{ \frac{C_q}{K} \int_{y_a}^{y} \sqrt{\frac{\rho_\infty}{\rho}}\, \frac{dy}{y} + \sqrt{\frac{C_f}{2} + C_q \left(\frac{u_a}{u_\infty} - \frac{u_w}{u_\infty} \right)} \right\}^2 - \frac{C_f}{2C_q} \qquad (12)$$

where again the integration can be performed numerically and where the subscript "a" refers to the matching point which was tentatively taken as equal to $y^+ \cong 50$. The constant k was assumed equal to 0.4 the non-blowing incompressible value. The velocity profile based on Equation (12) agrees very closely with the experimental profile in the range $30 \leq y^+ \leq 100$. The deviation from the experiment is +5 percent at $y^+ = 30$ and -5 percent at $y^+ = 100$. The deviation near the outer edge of the boundary layer is similar to the "velocity defect" found in incompressible turbulent boundary layers. Figure 21 illustrates these results with a typical set of u^+ versus y^+ profiles.

32. The non-dimensional velocities at the point of intersection i.e., u^+_i are shown plotted in Figure 22 against T_w/T_∞, the parameter suggested by Equation (10). No trend is indicated. The measurements when plotted against C_q show only the slightest dependence on blowing rate. See Figure 23.

SUMMARY AND CONCLUDING REMARKS

33. The compressible turbulent boundary layer on a porous flat plate with air injection has been studied experimentally in the Naval Ordnance Laboratory Hypersonic Tunnel No. 4. Velocity and temperature boundary-layer profiles were obtained at a Mach number of 5.1, Reynolds number of 1.5×10^7 per meter, T_w/T_∞ of 4.2 and 5 and for rates of air injection from zero to 0.08 percent of free-stream mass flow ($.0008\ \rho_\infty u_\infty$). Experimental values of skin friction were obtained from the velocity profiles.

34. As expected, the boundary-layer parameters, thickness (δ), displacement thickness (δ^*), momentum thickness (Θ), and the

velocity profile exponent (1/n) increase with rate of injection and the skin friction (C_f) decreases.

35. Comparison of the skin-friction coefficient with theories of Rubesin (reference (k)) and Persh (reference (l)) were made and it was found that both predicted the non-blowing C_f for the down-stream station. Rubesin's, however, predicted the trend with blowing within $\pm$ 25 percent, while Persh's theory was consistantly lower than the experiment, with the maximum being 50 percent.

36. The total temperature profiles showed that the Crocco profile describes the experimental data within about 8 percent of T or T_o, but, a closer examination of the data shows certain discrepancies between the total temperature profile and the theoretical profile.

37. The theoretical velocity profile as used in Rubesin's analysis has been examined. The empirical formula for the velocity at the interface between the laminar sublayer and the turbulent outer portion does not properly describe the interface location. In fact, the formula indicates u_i exceeds the free-stream velocity. The same differential equations for the velocity profile used in Rubesin's analysis were integrated numerically and fitted to the experimental data. The trend of the outer turbulent portion seems adequately described by this method within $\pm$ 5 percent in the range $30 \leq y^+ \leq 100$. The resulting interface velocity u_i^+ was about 14 ± 3 independent of changes in T_w/T_∞ and showed a very slight dependence on C_q.

38. The above represents the first results of a larger program intended to extend the basic knowledge of the mass-transfer phenomena in a systematic way. The present results are too limited in the range of the variables investigated and more tests are needed to establish and extend the trends with injection rate, heat transfer, and Reynolds number. To accomplish this, an extensive program is planned incorporating needed improvements, as for example, a porous insert with a more uniform injection rate, instrumented for measuring local heat transfer and static pressure at the surface, a cooling system adequate for a wider range of controlled temperatures, and refined instrumentation to resolve the questions concerning the region near the surface. Ultimately, mass addition should be investigated at higher Mach numbers with various injected gases, and under pressure gradient conditions.

REFERENCES

(a) Mickley, H. S., Ross, R. C., Squyers, A. L., and Stewart, W. E., "Heat, Mass and Momentum Transfer for Flow Over a Flat Plate with Blowing or Suction," NACA TN 3208, July 1954

(b) Leadon, B. M., and Scott, C. J., "Measurement of Recovery Factors and Heat Transfer Coefficients with Transpiration Cooling in a Turbulent Boundary Layer at M=3.0 Using Air and Helium as Coolants." Research Report 126 Inst. of Tech., University of Minnesota, Feb 1956

(c) Rubesin, M. W., Pappas, C. C., Okuno, A. F., "The Effect of Fluid Injection on the Compressible Turbulent Boundary Layer - Preliminary Tests on Transpiration Cooling of a Flat Plate at M=2.7 with Air as the Injected Gas." NACA RM A55119, 1955

(d) Pappas, C. C., "Effect of Injection of Foreign Gases on the Skin Friction and Heat Transfer of the Turbulent Boundary Layer." Paper 59-78 presented at 27th Annual Meeting IAS Jan 1959

(e) Winkler, E. M., and Cha, M. H., "Experimental Investigations of the Effect of Heat Transfer on Hypersonic Turbulent Boundary-Layer Skin Friction." NAVORD Report 6631, 1959

(f) Winkler, E. M., "Stagnation Temperature Probes for Use at High Supersonic Speeds and Elevated Temperatures." NAVORD Report 3834, 1954

(g) Wegener, P., "Summary of Recent Experimental Investigations in the NOL Hypersonic Wind Tunnel." Journal of the Aero. Sci. Vol 18 No. 10 p 665, Oct 1951

(h) Wegener, P. and Lobb, R. K., "An Experimental Study of Hypersonic Wind Tunnel Diffuser," Journal of the Aero. Sci. Vol 20 No. 2 p 105, Feb 1953

(i) Ames Research Staff, "Equations, Tables, and Charts for Compressible Flow," NACA Report 1135, 1953

(j) Lobb, R. K., Winkler, E. M., and Persh, J., "NOL Hypersonic Tunnel No. 4 Results VII: Experimental Investigation of Turbulent Boundary Layers in Hypersonic Flow," NAVORD Report 3880, March 1955

REFERENCES

(k) Rubesin, M. W., "An Analytical Estimation of the Effect of Transpiration Cooling on the Heat-Transfer and Skin-Friction Characteristics of a Compressible Turbulent Boundary Layer," NACA TN 3341, Dec 1954

(l) Persh, J., "A Theoretical Investigation of the Effect of Injection of Air on Turbulent Boundary-Layer Skin-Friction and Heat-Transfer Coefficients at Supersonic and Hypersonic Speeds." NAVORD Report 4220, Jan 1957 (Declassified 14 May 1959)

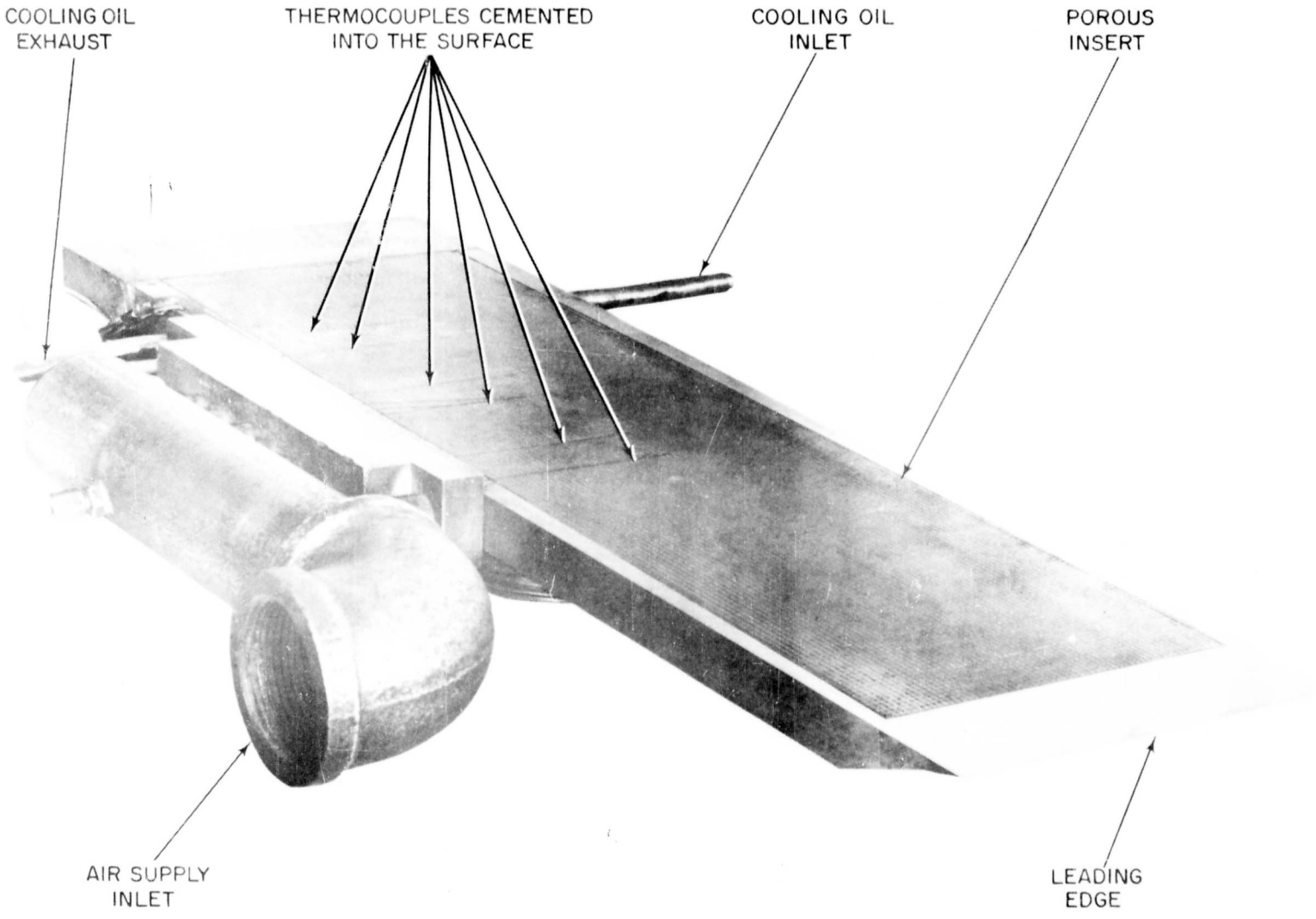

FIG.1 TOP VIEW OF POROUS PLATE

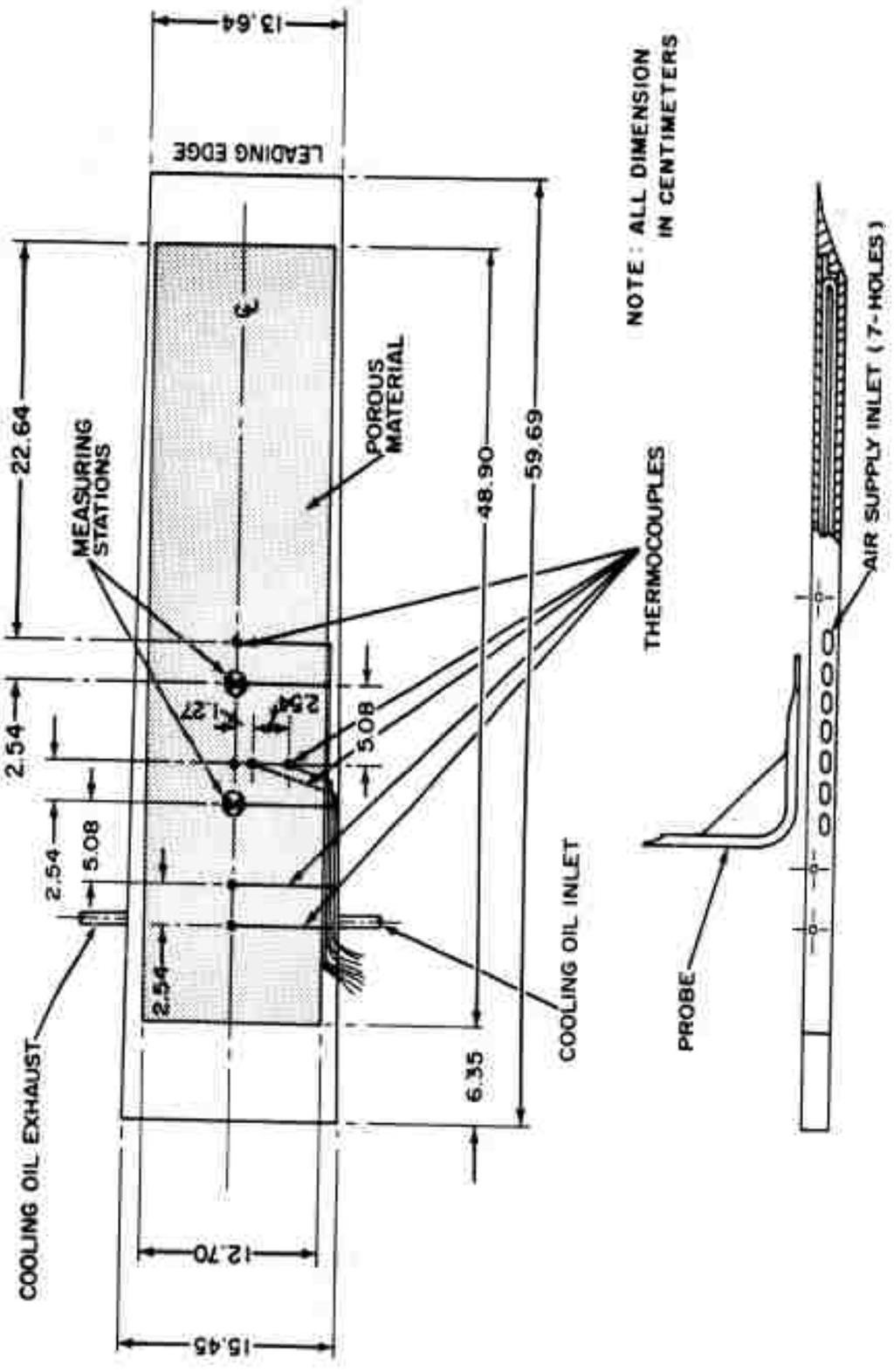

FIG.2 SKETCH OF MODEL

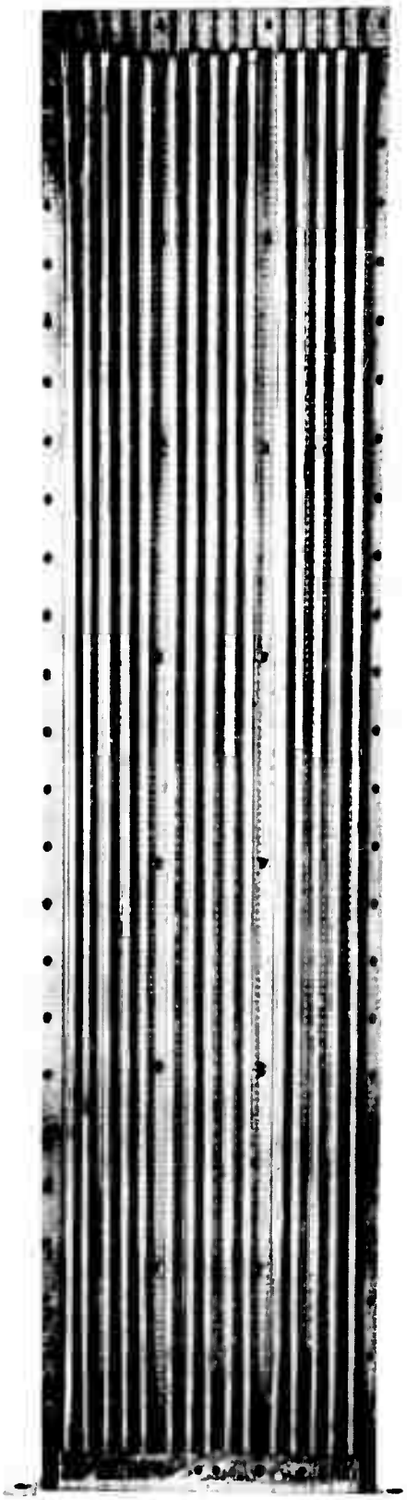

FIG. 3 UNDERSIDE OF POROUS INSERT SHOWING COOLING TUBES

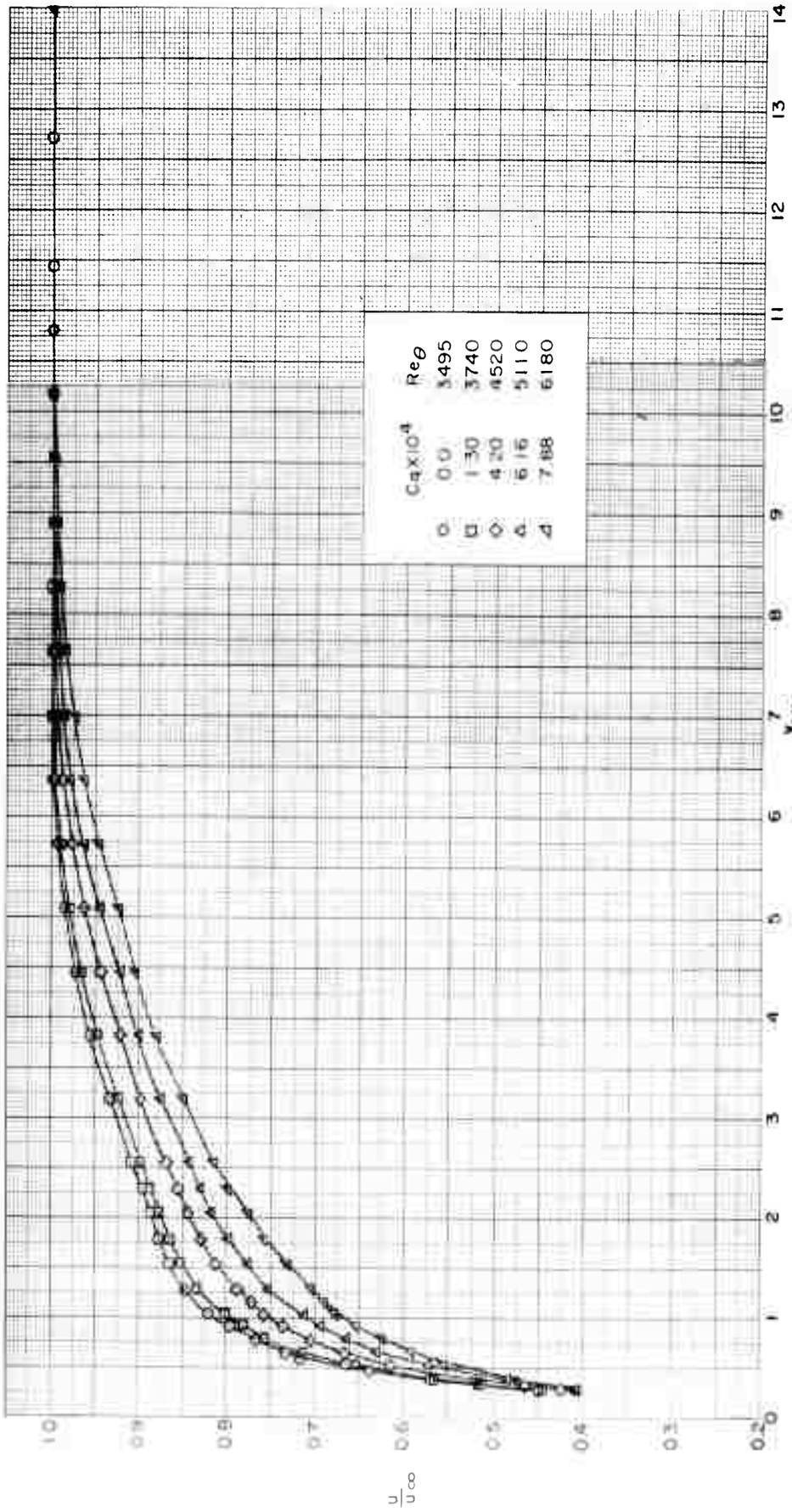

FIG. 4 TURBULENT BOUNDARY-LAYER VELOCITY PROFILE WITH VARIOUS RATES OF AIR INJECTION

$Re_x = 4.3 \times 10^6$, $T_w/T_\infty = 5.04$

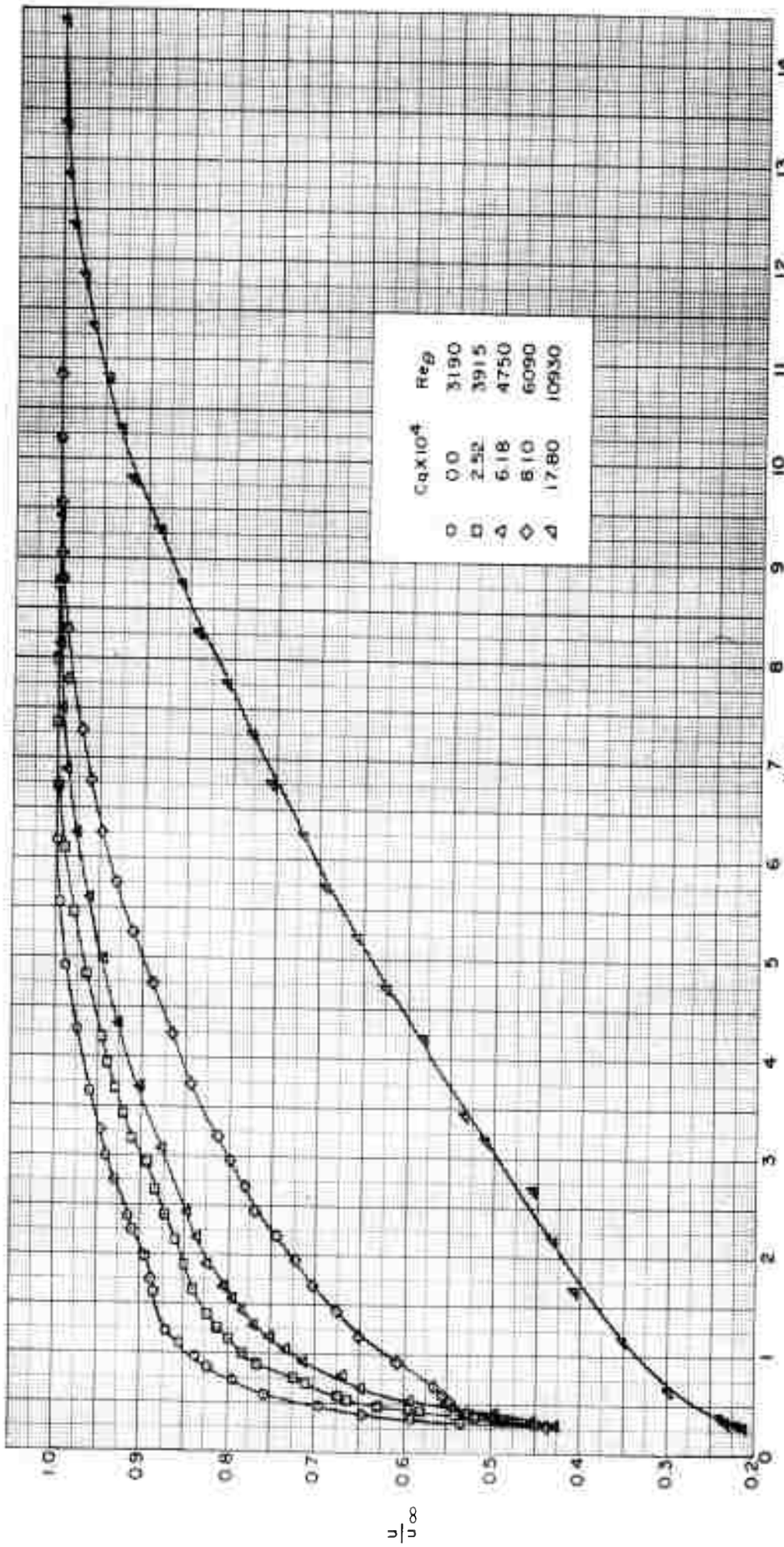

FIG. 5 TURBULENT BOUNDARY-LAYER VELOCITY PROFILE WITH VARIOUS RATES OF AIR INJECTION
$Re_x = 4.2 \times 10^6$, $T_w/T_\infty = 4.23$

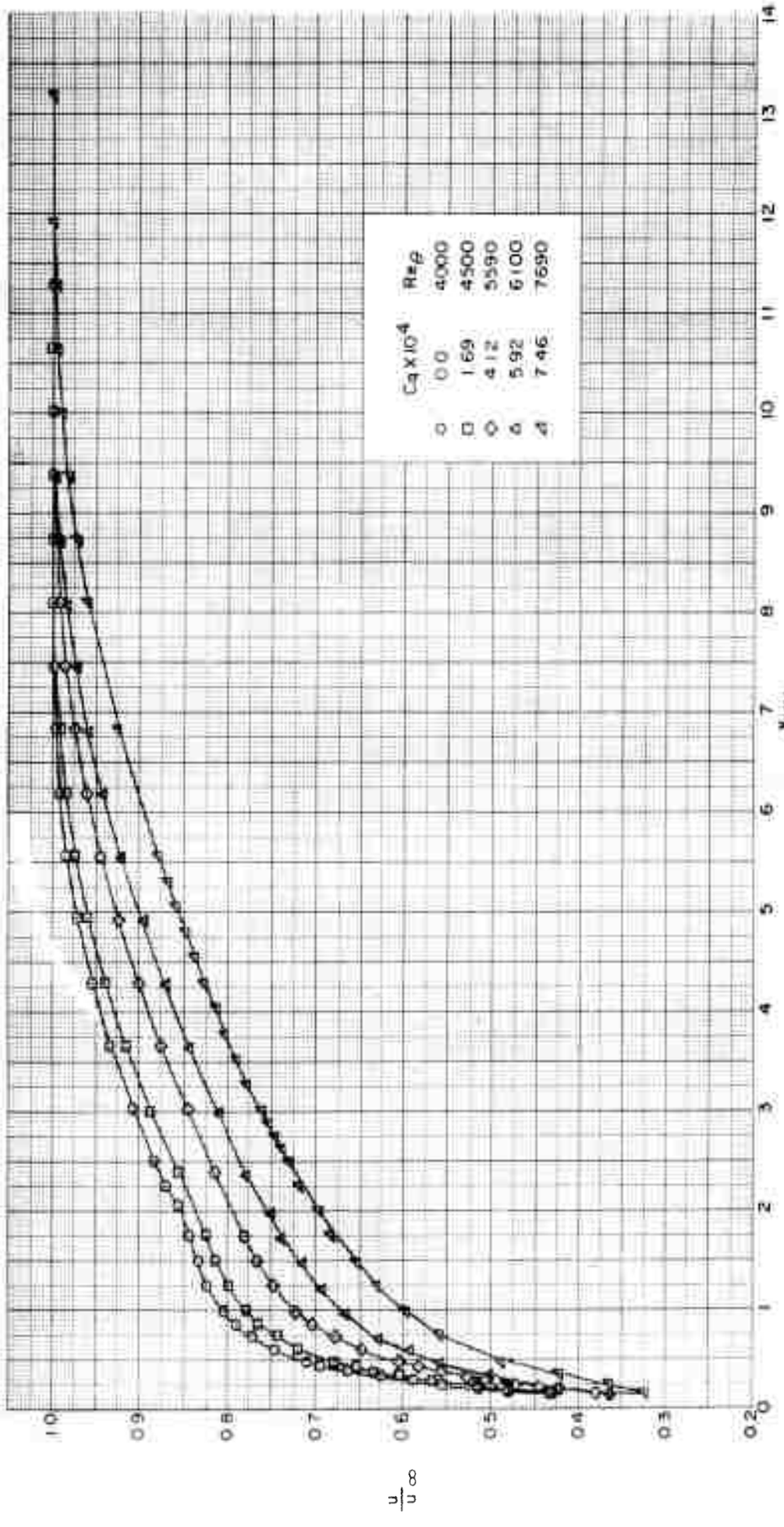

FIG.6 TURBULENT BOUNDARY-LAYER VELOCITY PROFILE WITH VARIOUS RATES OF AIR INJECTION
$Re_x = 5.5 \times 10^6$, $T_w / T_\infty = 5.04$

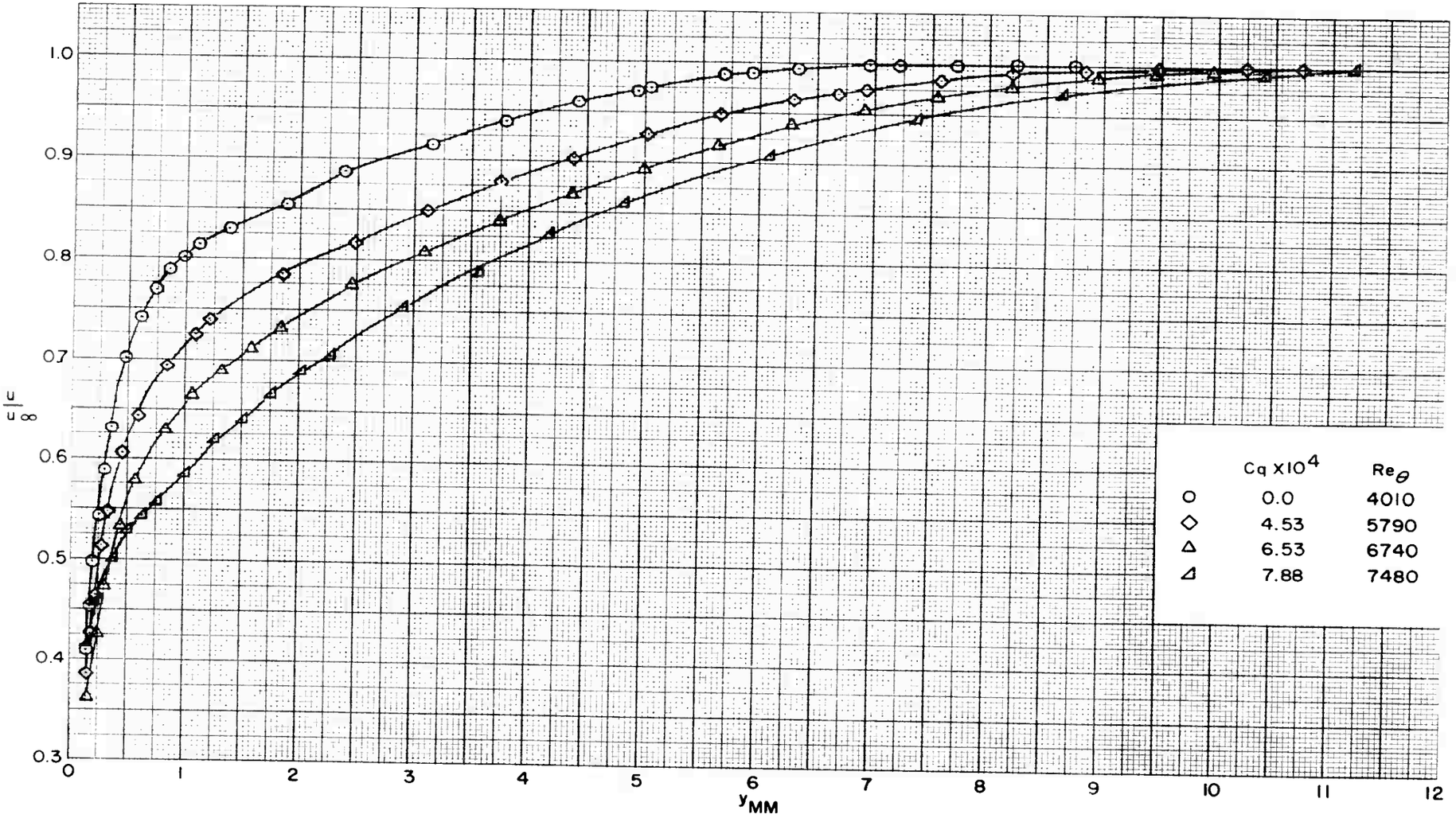

FIG. 7 TURBULENT BOUNDARY-LAYER VELOCITY PROFILE WITH VARIOUS RATES OF AIR INJECTION

$Re_x = 5.4 \times 10^6$ $T_w / T_\infty = 4.23$

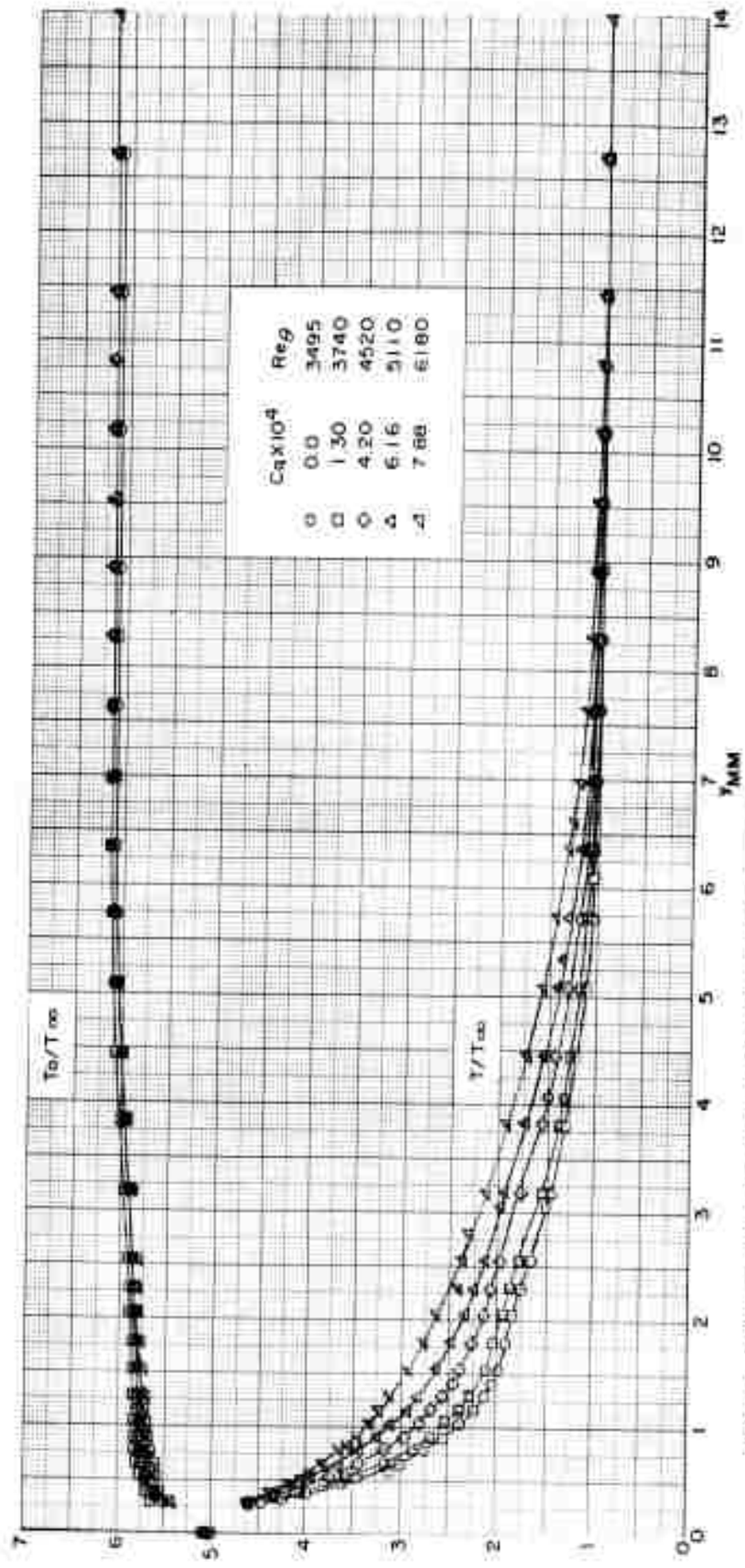

FIG. 8 TURBULENT BOUNDARY-LAYER TOTAL AND STATIC TEMPERATURE PROFILES WITH VARIOUS RATES OF AIR INJECTION
$Re_x = 4.3 \times 10^6$, $T_w / T_\infty = 5.04$

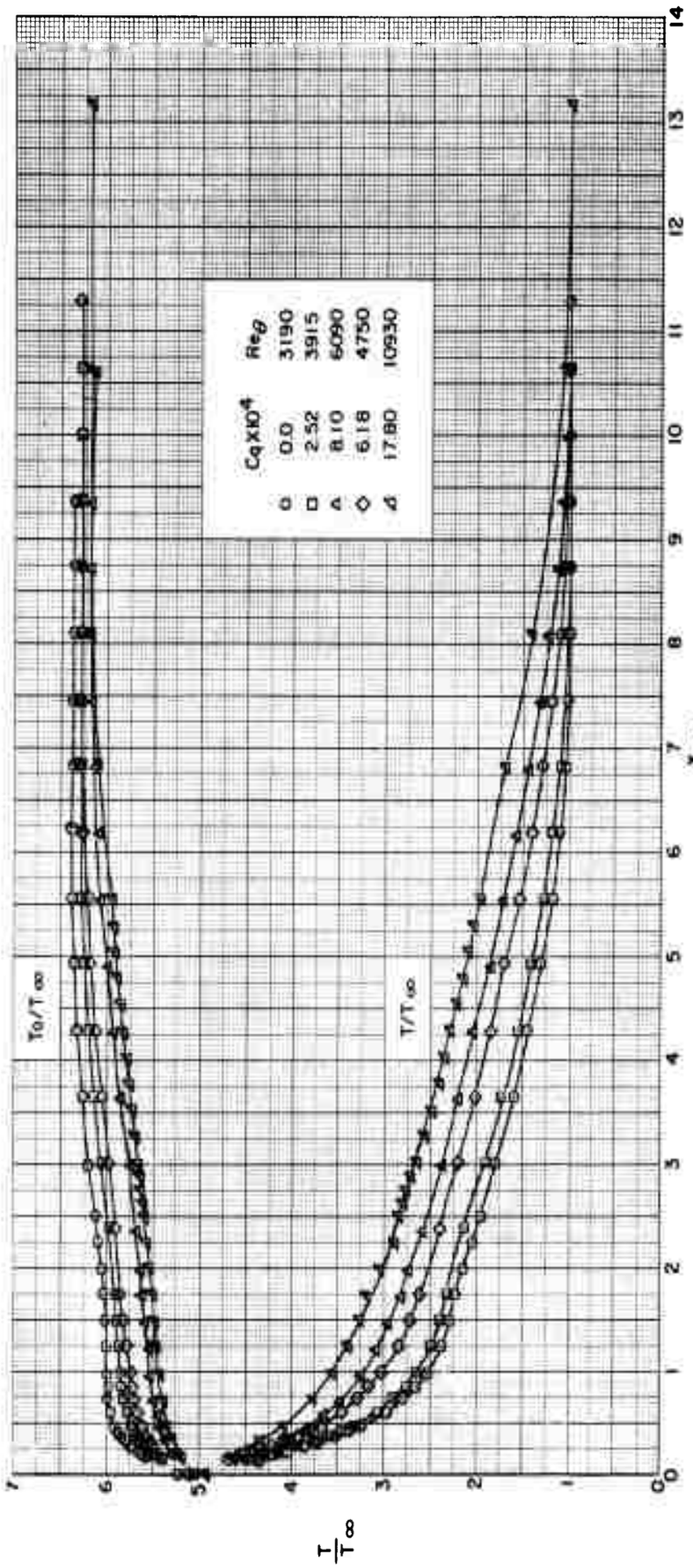

FIG. 9 TURBULENT BOUNDARY-LAYER TOTAL AND STATIC TEMPERATURE PROFILES WITH VARIOUS RATES OF AIR INJECTION

$Re_x = 4.2 \times 10^6$, $T_w/T_\infty = 4.23$

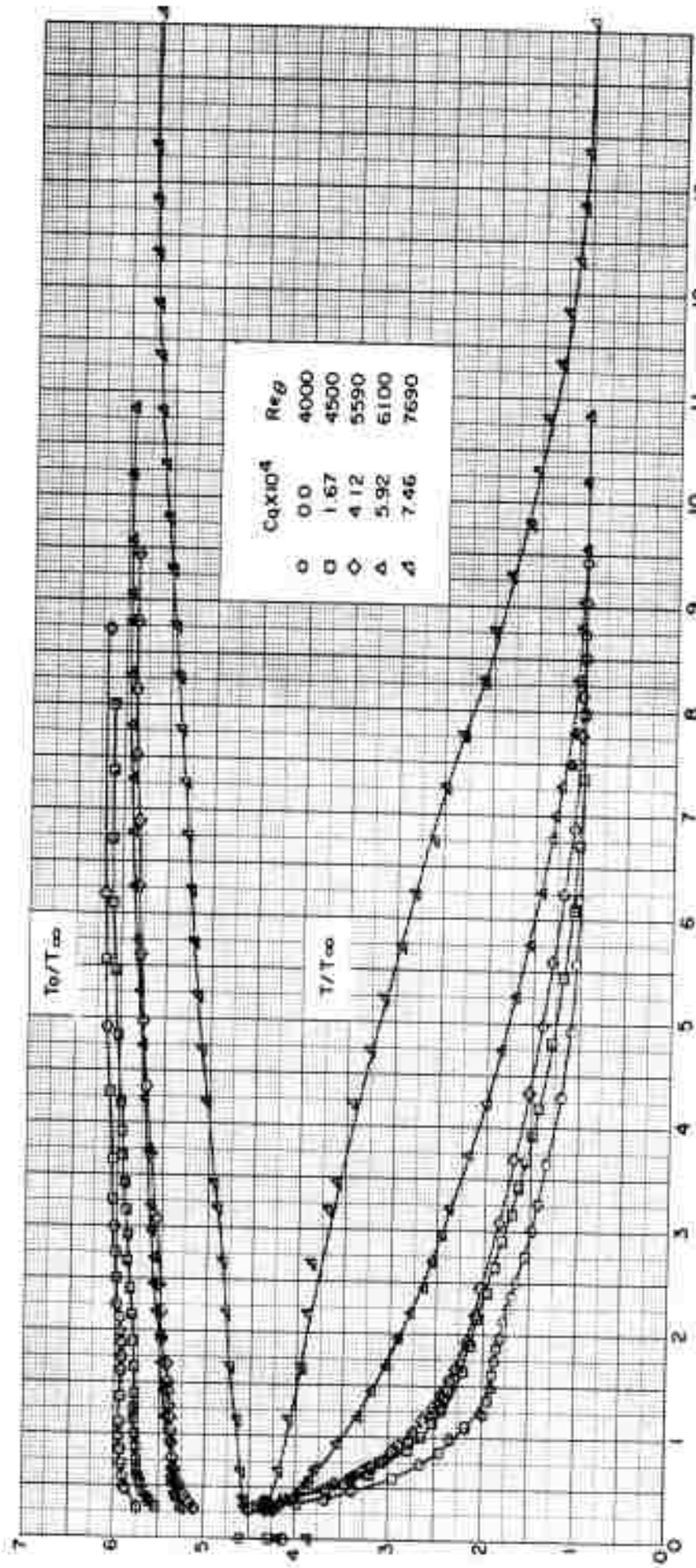

FIG.10 TURBULENT BOUNDARY-LAYER TOTAL AND STATIC TEMPERATURE PROFILES WITH VARIOUS RATES OF AIR INJECTION

$Re_X = 5.5 \times 10^6$, $T_W/T_\infty = 5.04$

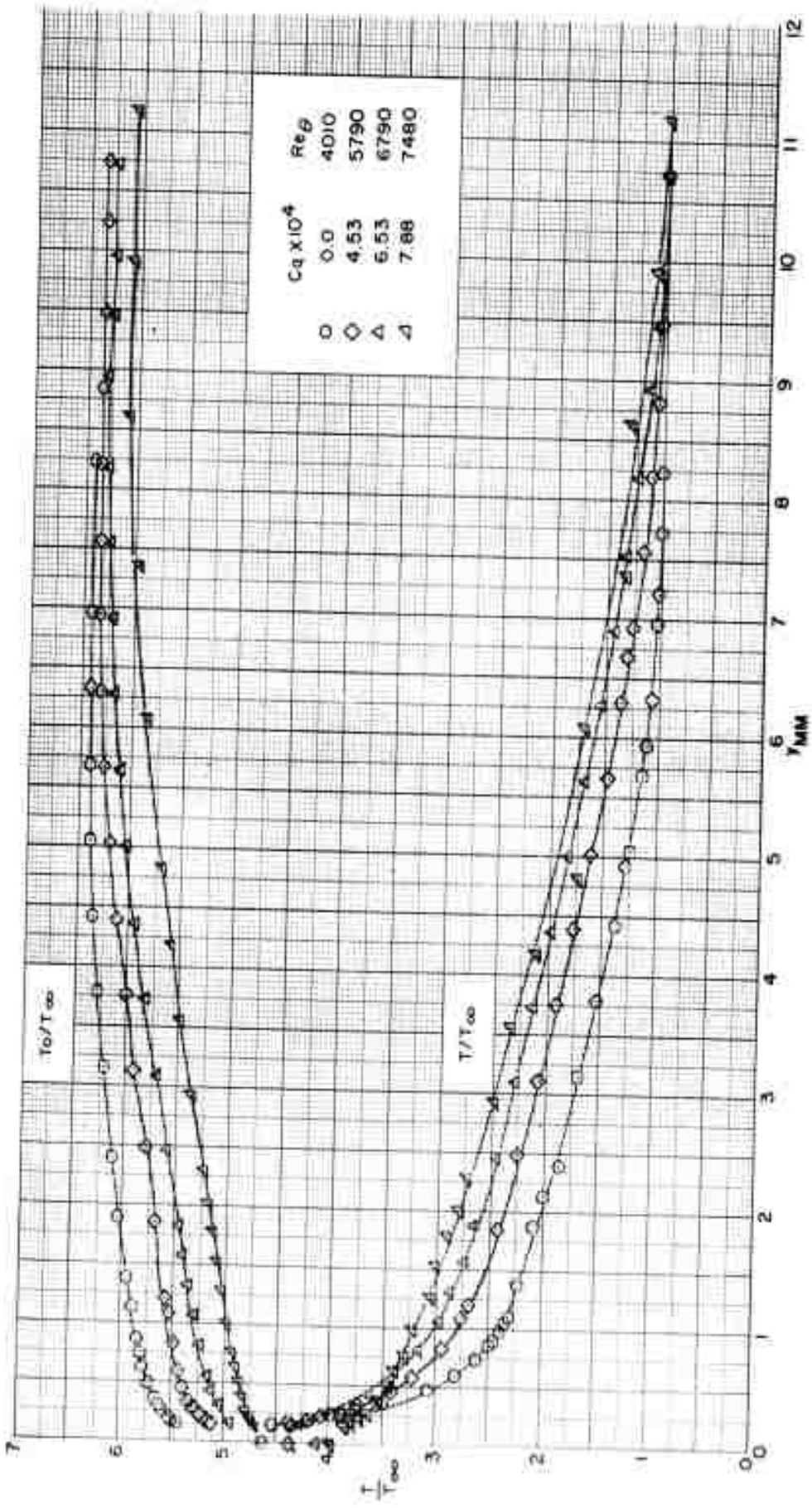

FIG. 11 TURBULENT BOUNDARY-LAYER TOTAL AND STATIC TEMPRATURE PROFILES WITH VARIOUS RATES OF AIR INJECTION
$Re_x = 5.4 \times 10^6$ $T_w/T_\infty = 4.23$

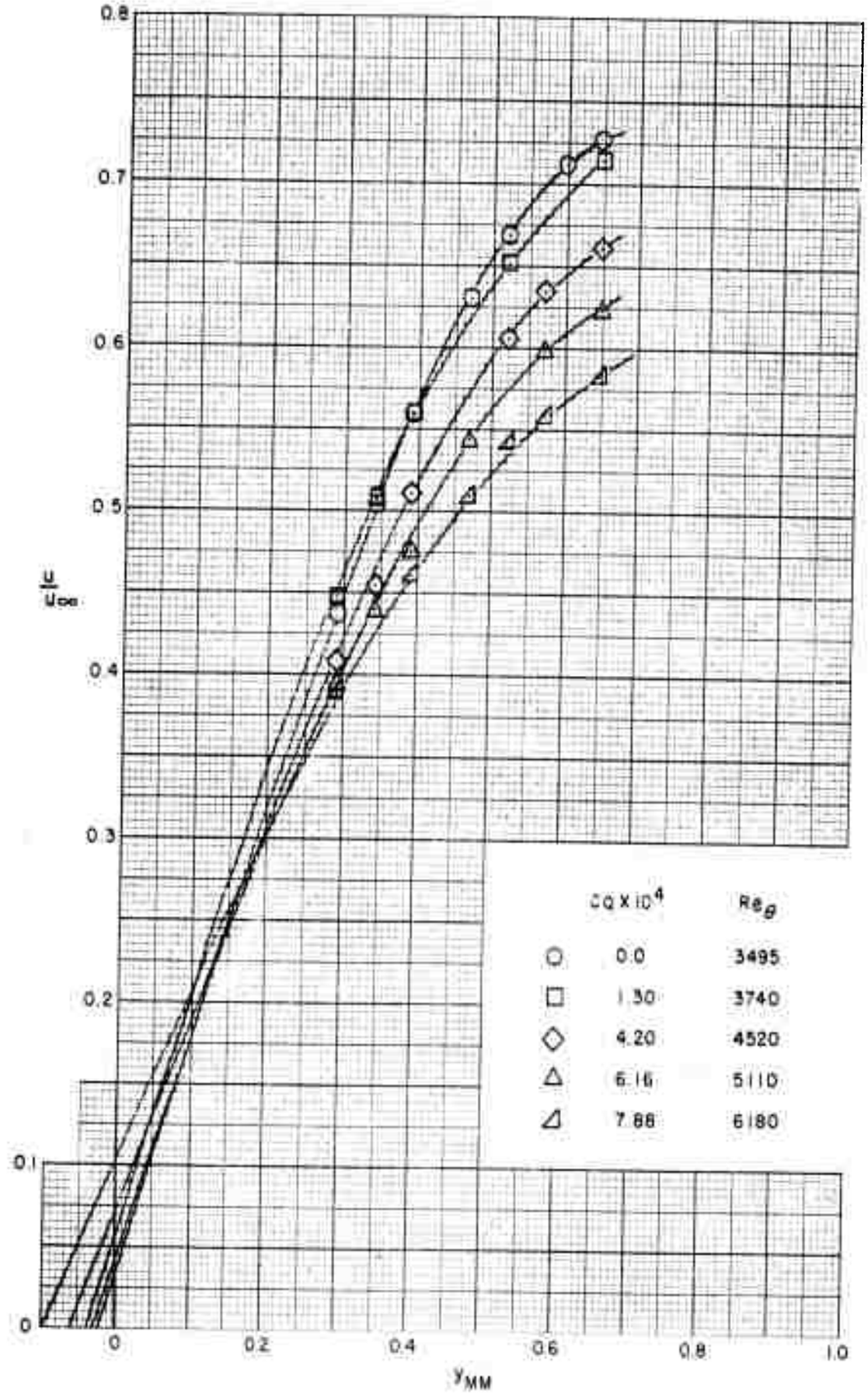

FIG. 12 DETAIL OF THE VELOCITY PROFILE, $y < 1.0$ MM
$Re_x = 4.3 \times 10^6$, $T_w/T_\infty = 5.04$

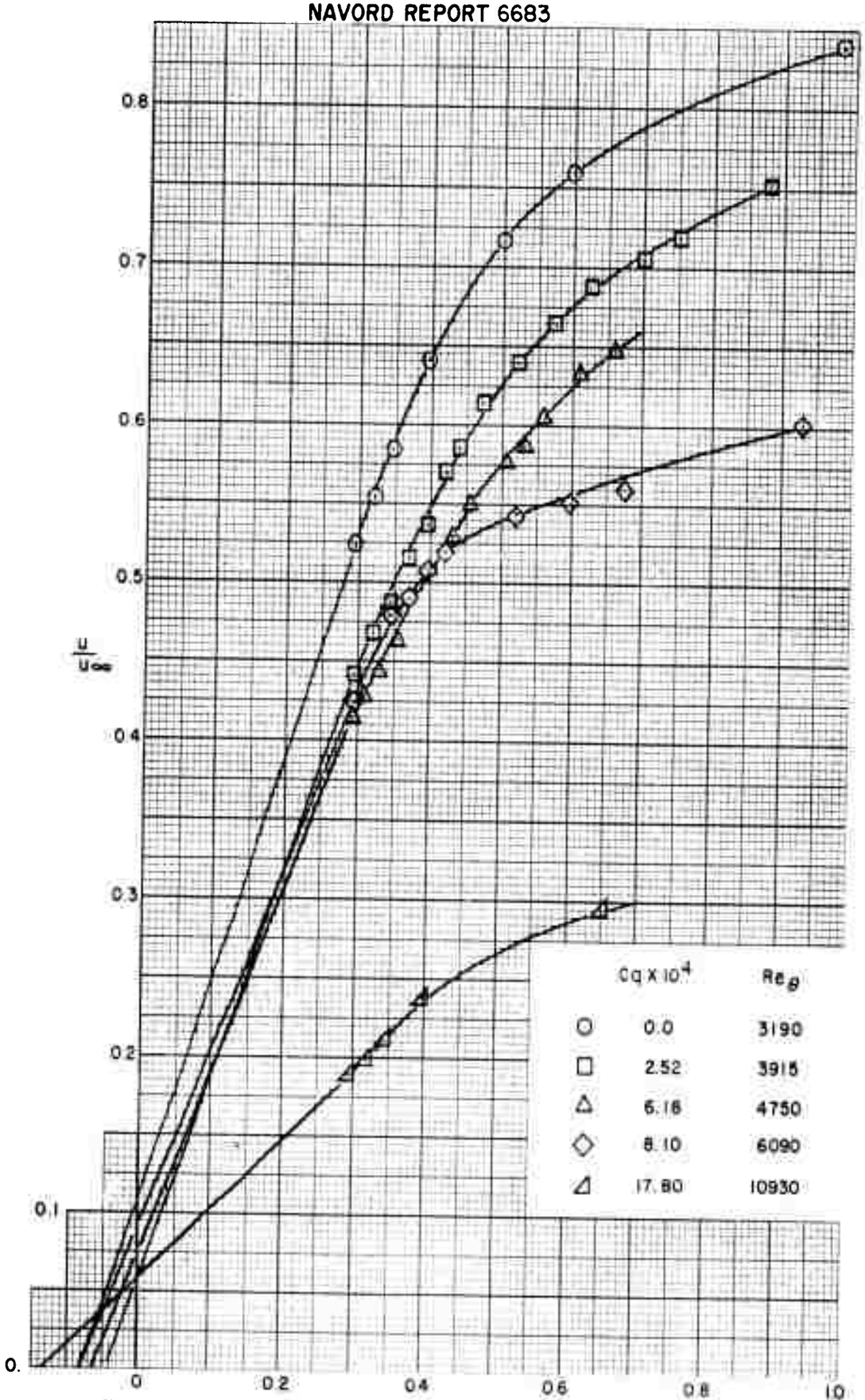

FIG. 13 DETAIL OF THE VELOCITY PROFILE, $y < 1.0$ MM

$Re_x = 4.2 \times 10^6$, $T_w/T_\infty = 4.23$

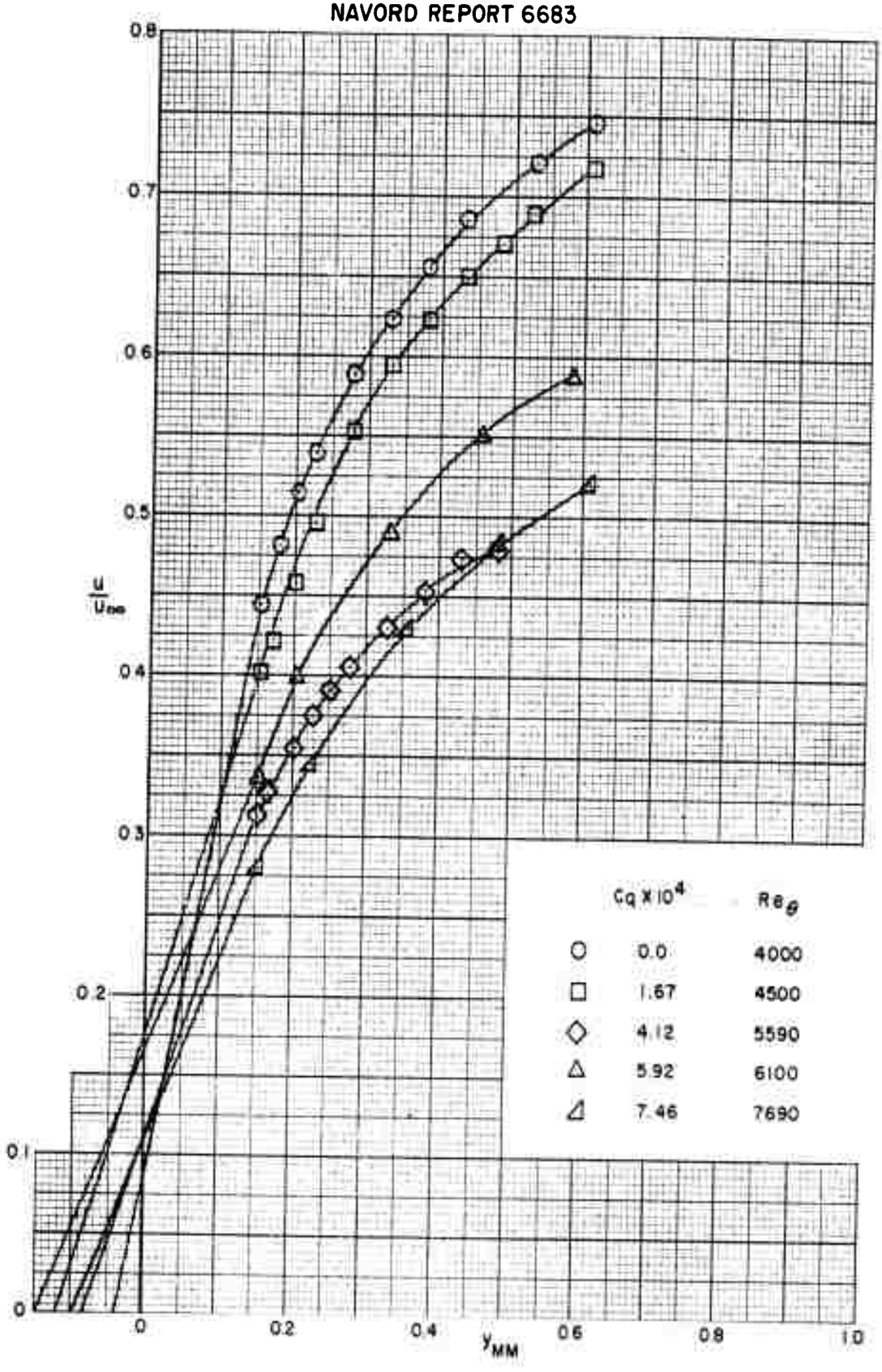

FIG. 14 DETAIL OF THE VELOCITY PROFILE, $y < 1.0$ MM
$Re_x = 5.5 \times 10^6$, $T_w/T_\infty = 5.04$

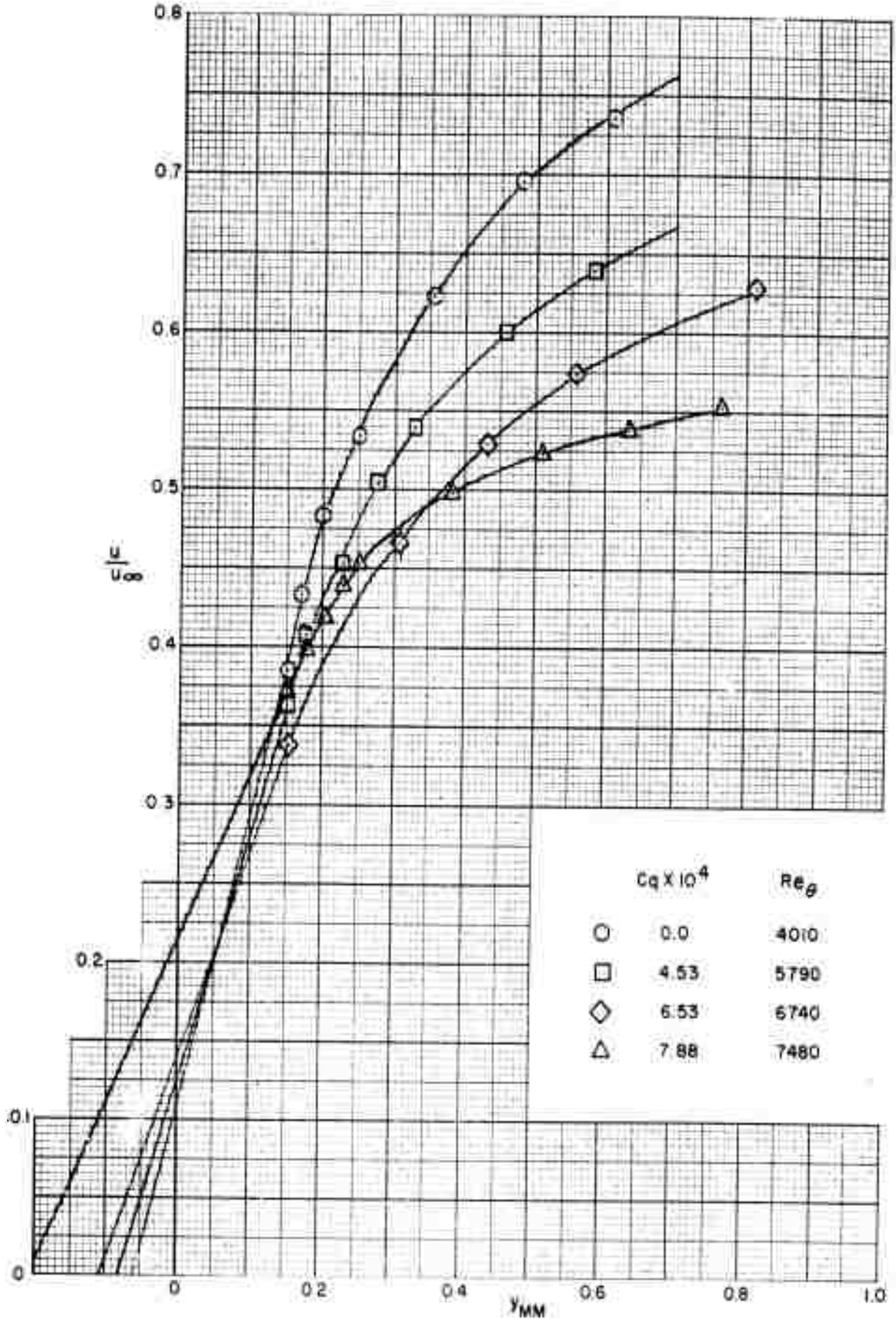

FIG. 15 DETAIL OF THE VELOCITY PROFILE, $y < 1.0$ MM
$Re_x = 5.4 \times 10^6$, $T_w/T_\infty = 4.23$

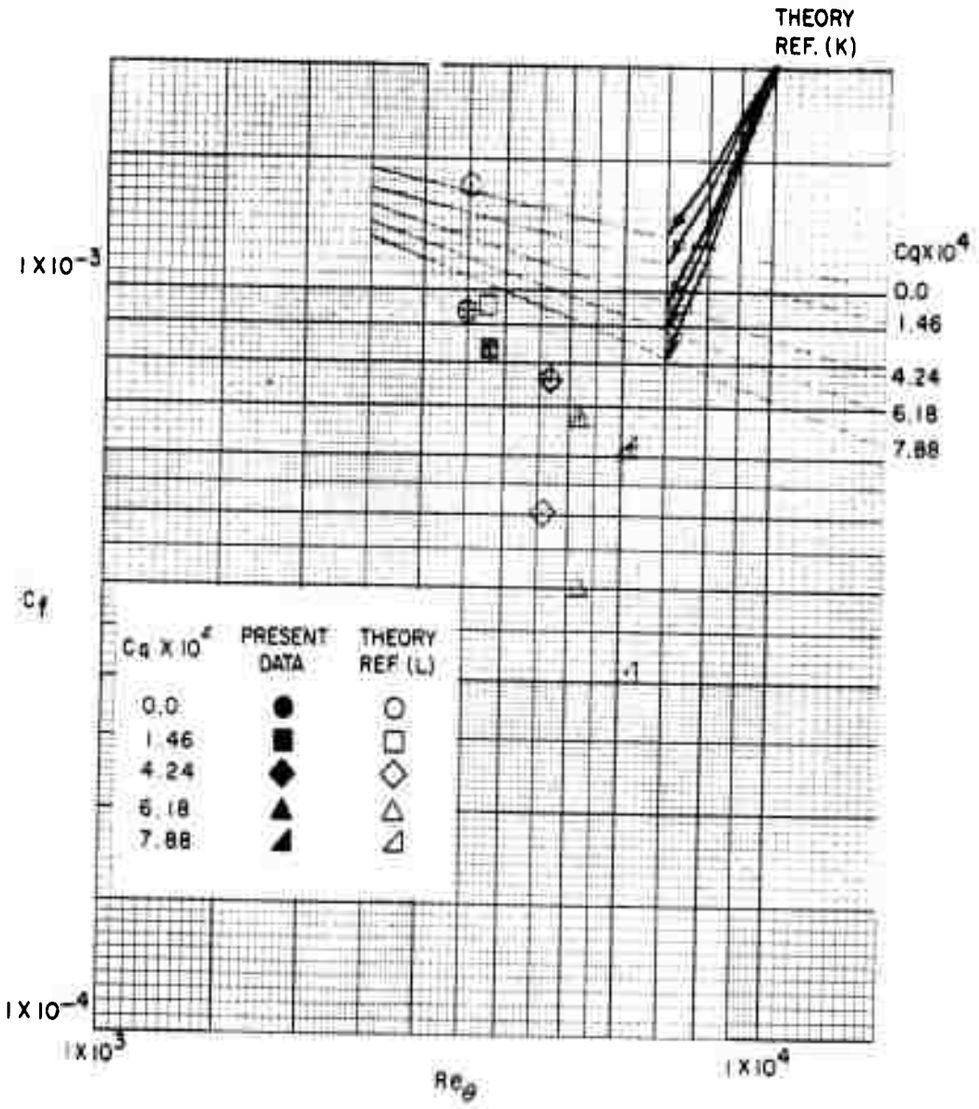

FIG. 16a SKIN-FRICTION COEFFICIENT VERSUS MOMENTUM THICKNESS REYNOLDS NUMBER
$Re_x = 4.3 X 10^6$ $T_w/T_\infty = 5.04$

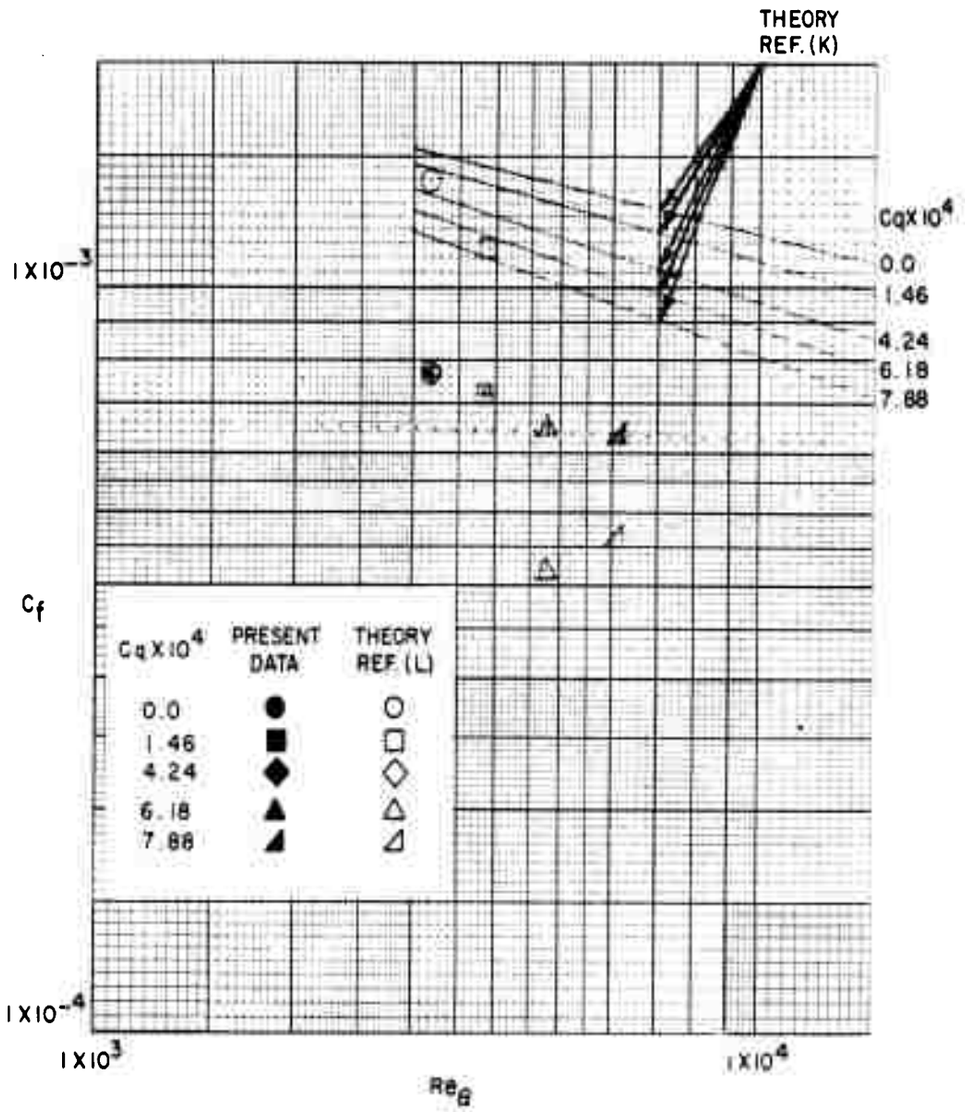

FIG. 16b SKIN-FRICTION COEFFICIENT VERSUS MOMENTUM THICKNESS REYNOLDS NUMBER
$Re_x = 4.2 \times 10^6$, $Tw/T\infty = 4.23$

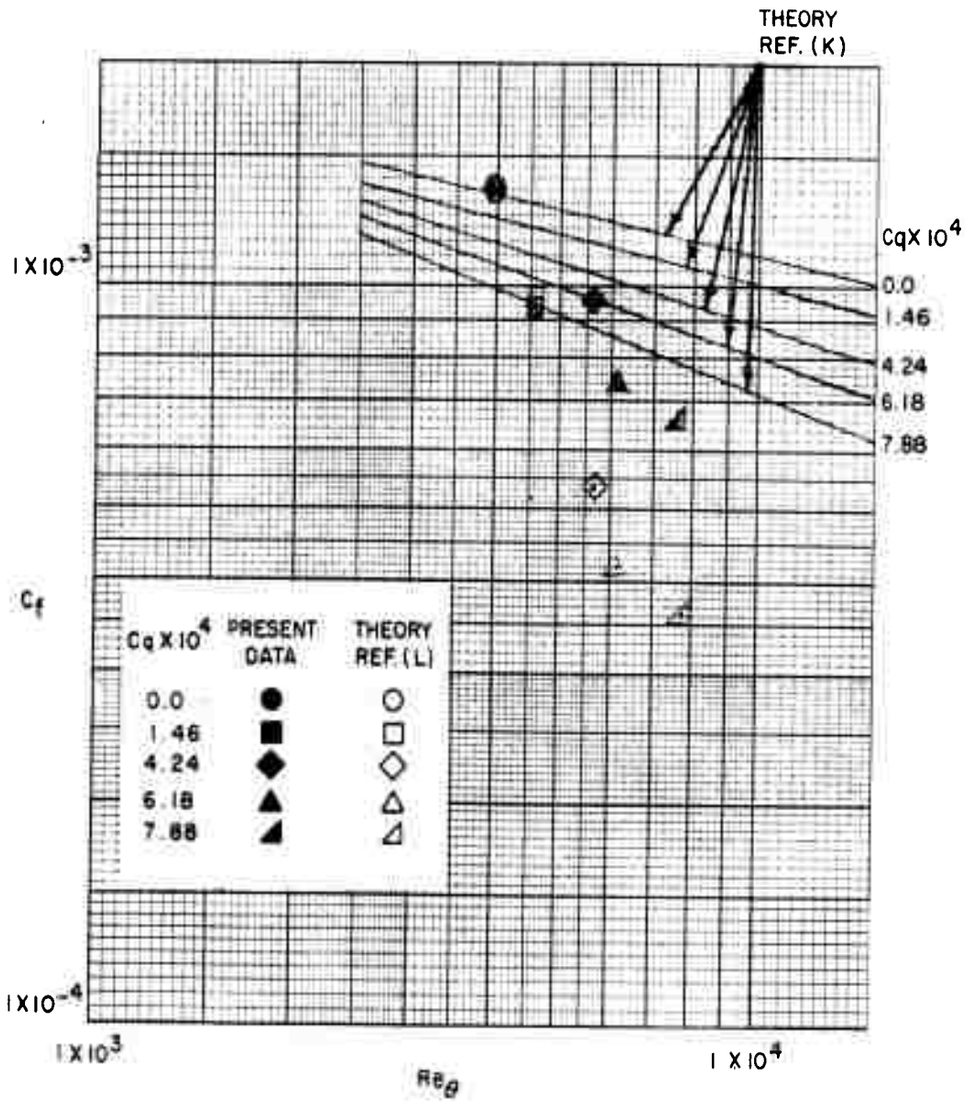

FIG. 17a SKIN-FRICTION COEFFICIENT VERSUS MOMENTUM THICKNESS REYNOLDS NUMBER

$Re_x = 5.5 \times 10^6$, $Tw/T\infty = 5.04$

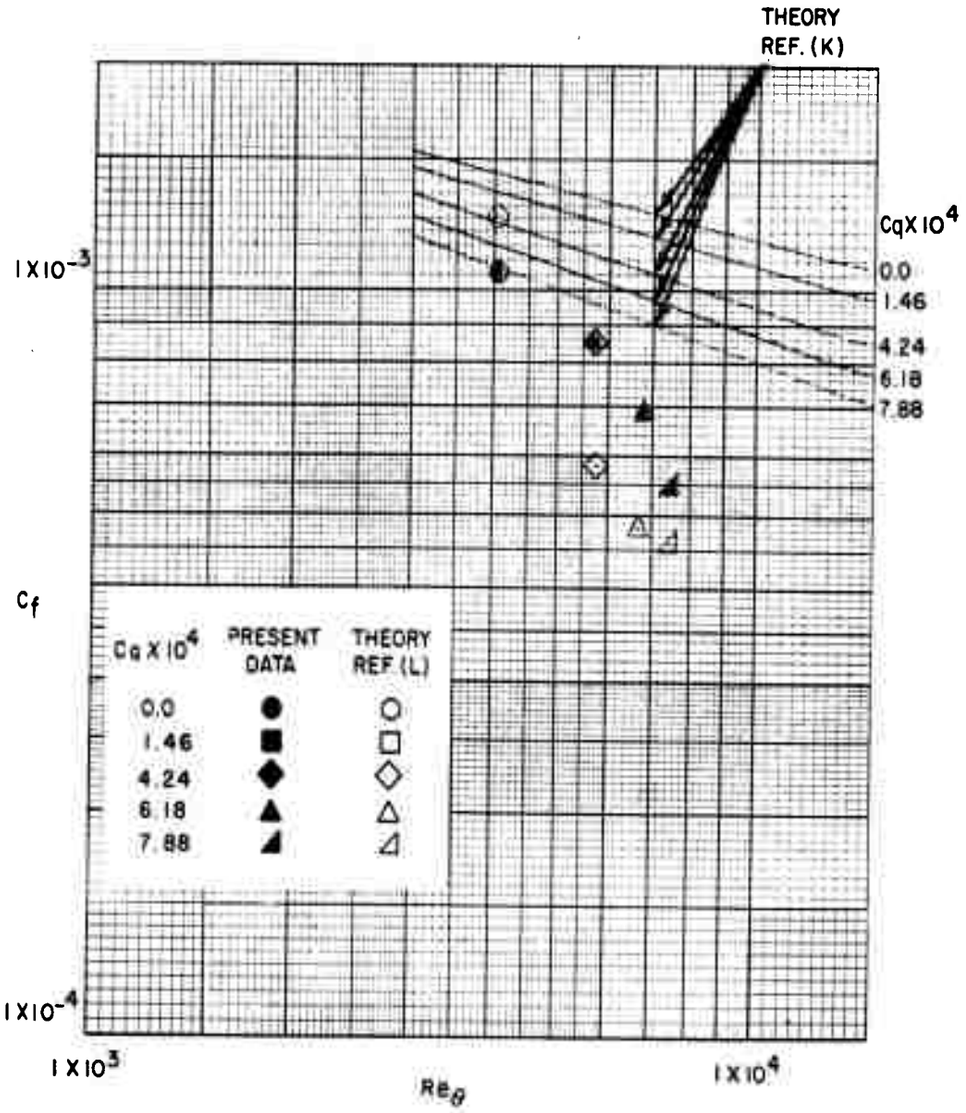

FIG. 17b SKIN-FRICTION COEFFICIENT VERSUS MOMENTUM THICKNESS REYNOLDS NUMBER

$Re_x = 5.4 \times 10^6$, $Tw/T\infty = 4.23$

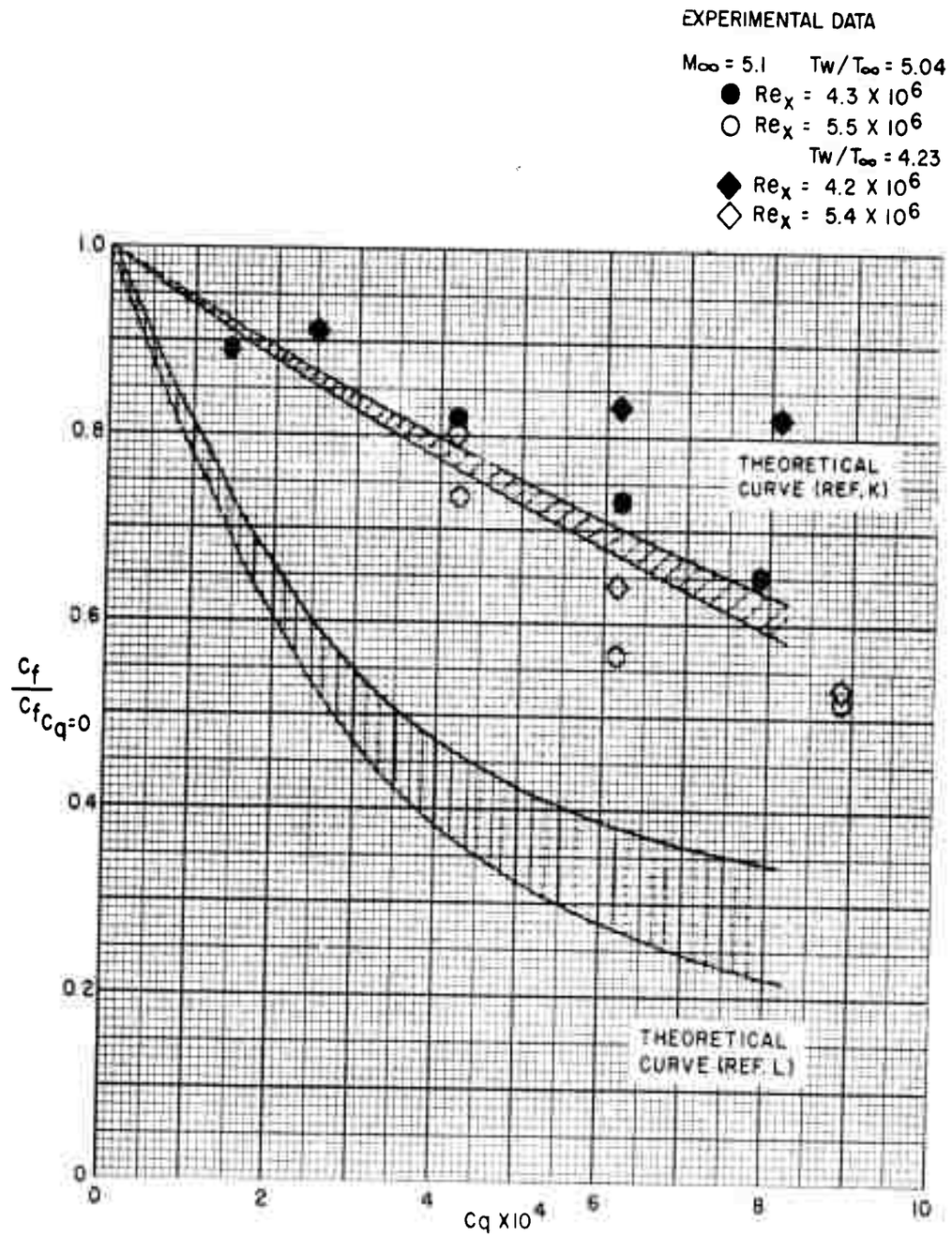

FIG.18 VARIATION OF SKIN-FRICTION RATIO WITH AIR INJECTION RATE ($C_{f_{C_q=0}}$ = SKIN-FRICTION COEFFICIENT FOR ZERO INJECTION RATE)

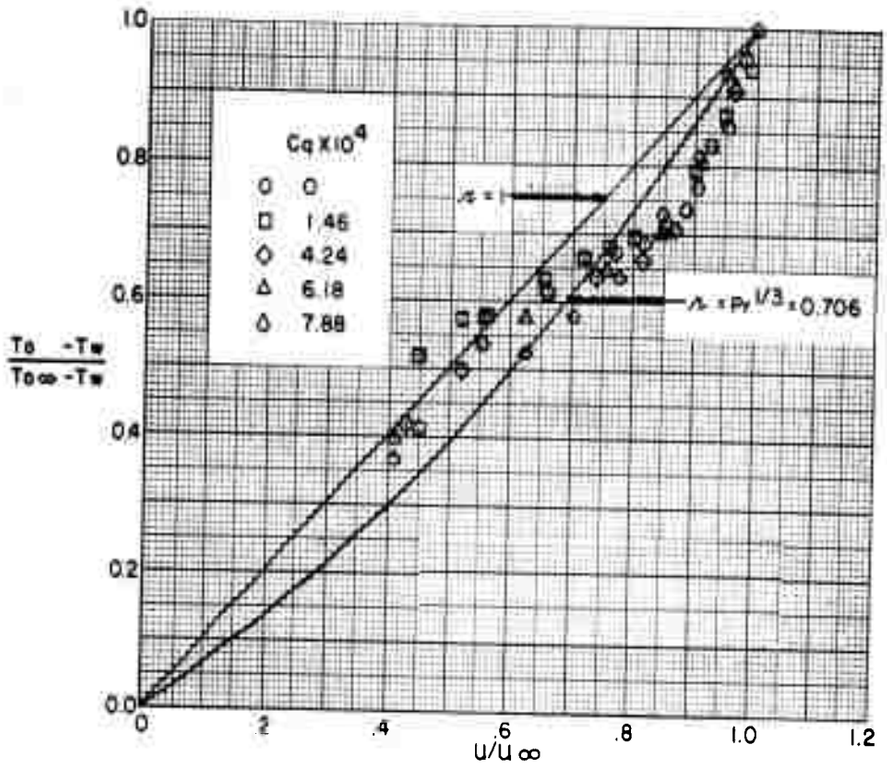

a. $T_w/T_\infty = 5.04$

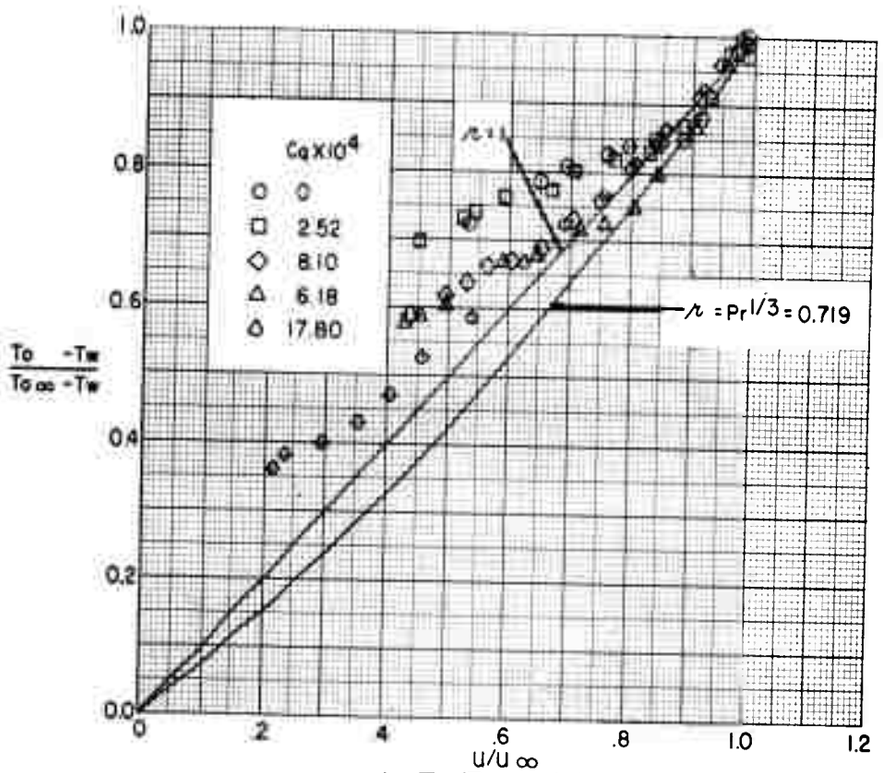

b. $T_w/T_\infty = 4.23$

FIG. 19 COMPARISON OF EXPERIMENTAL AND THEORETICAL TEMPERATURE-VELOCITY DISTRIBUTIONS
$M_\infty = 5.08$ $Re_x = 4.2 \times 10^6$

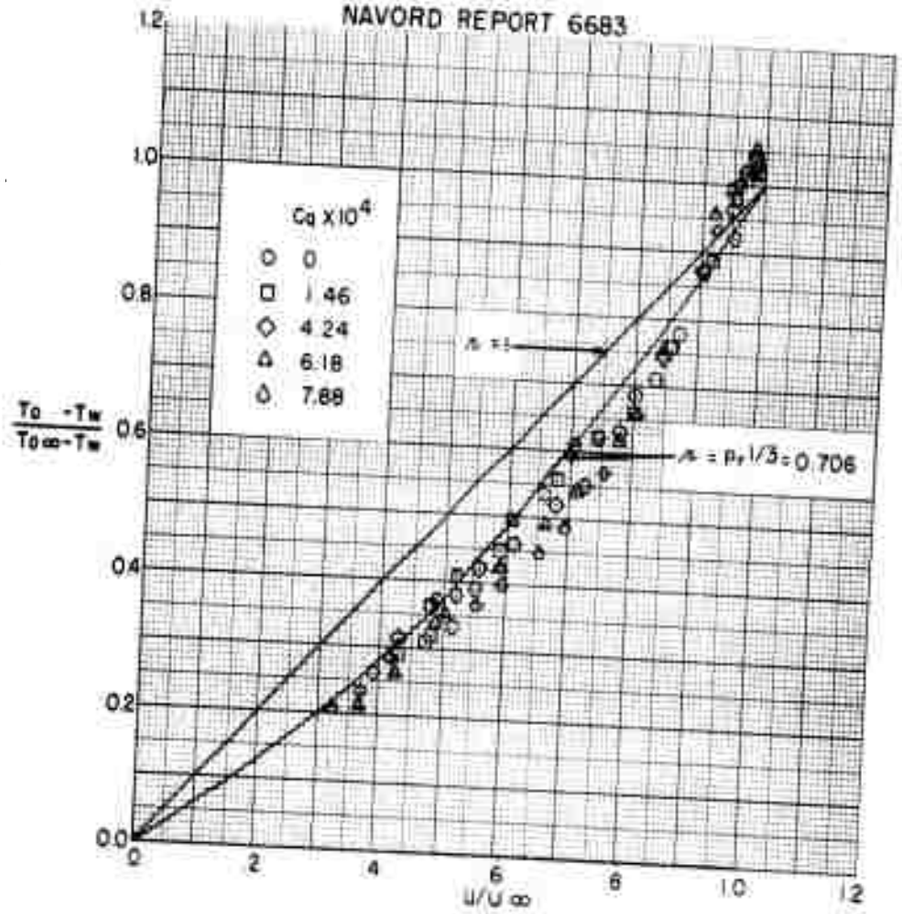

a. $T_w/T_\infty = 5.04$

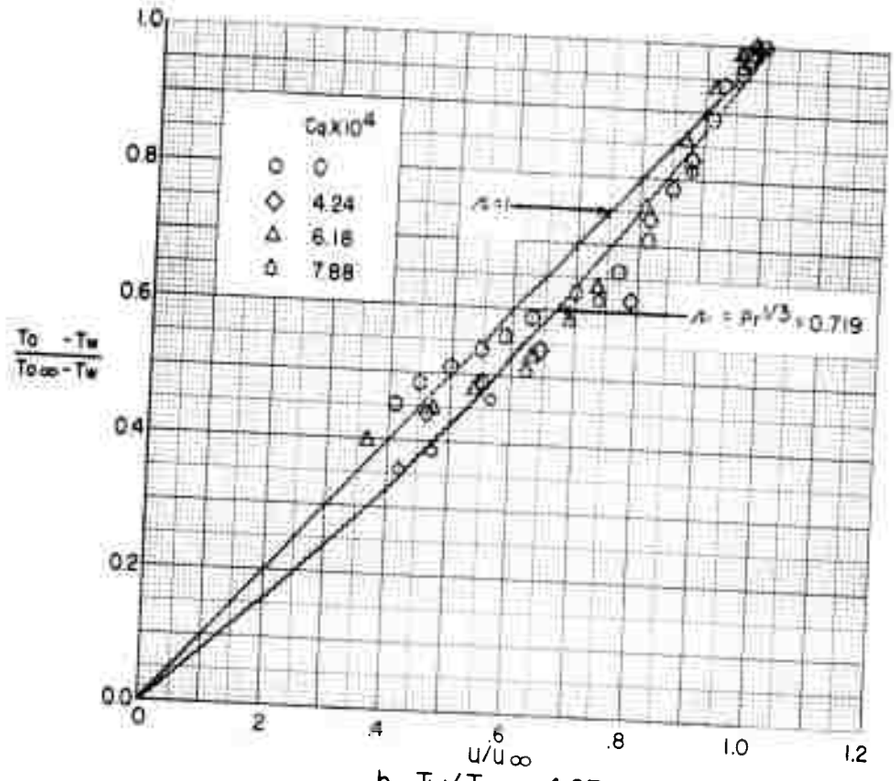

b. $T_w/T_\infty = 4.23$

FIG. 20 COMPARISON OF EXPERIMENTAL AND THEORETICAL TEMPERATURE-VELOCITY DISTRIBUTIONS
$M_\infty = 5.08$ $Re_x = 5.4 \times 10^6$

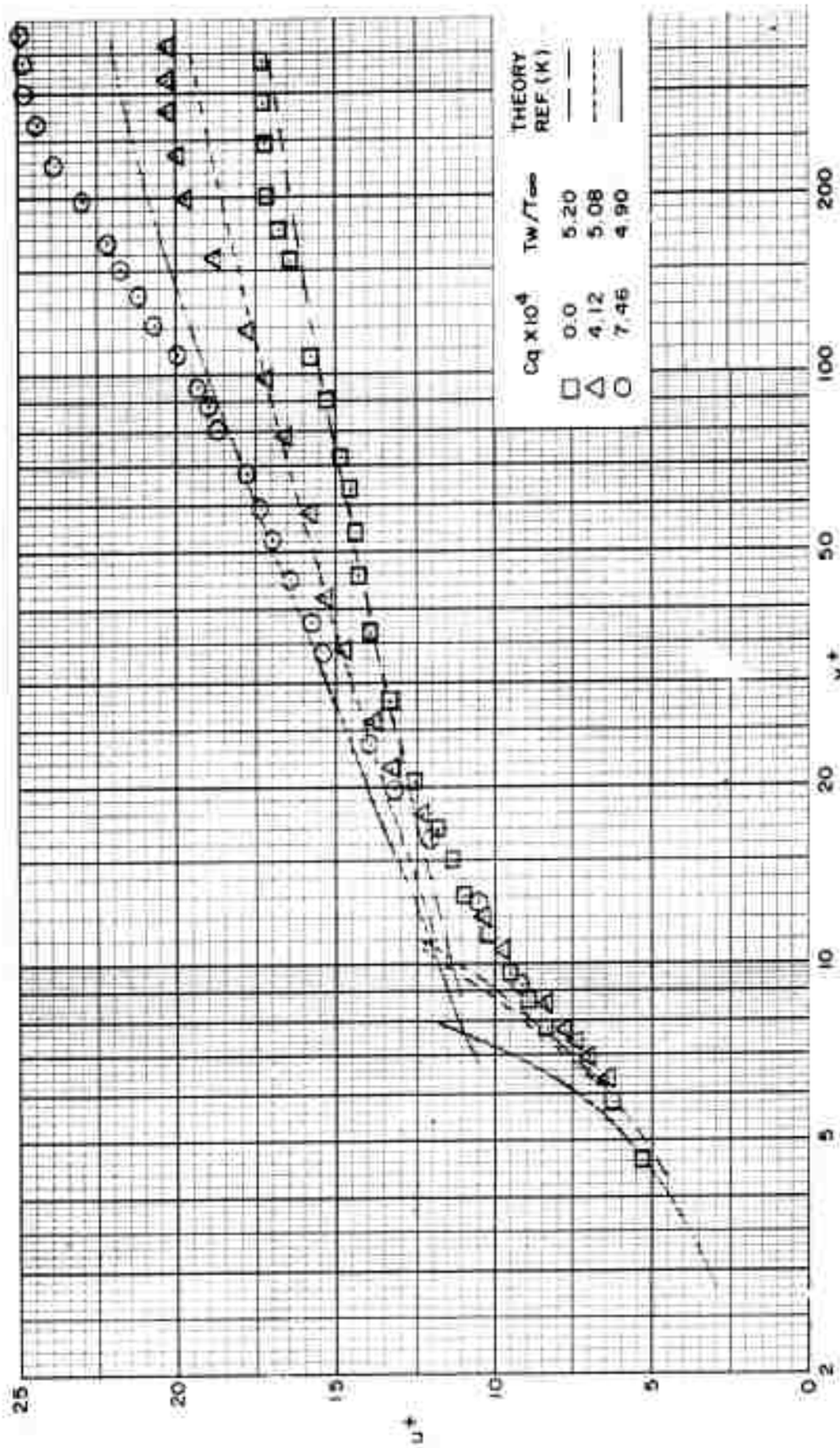

FIG. 21 COMPARISON OF EXPERIMENTAL AND THEORETICAL VELOCITY PROFILES

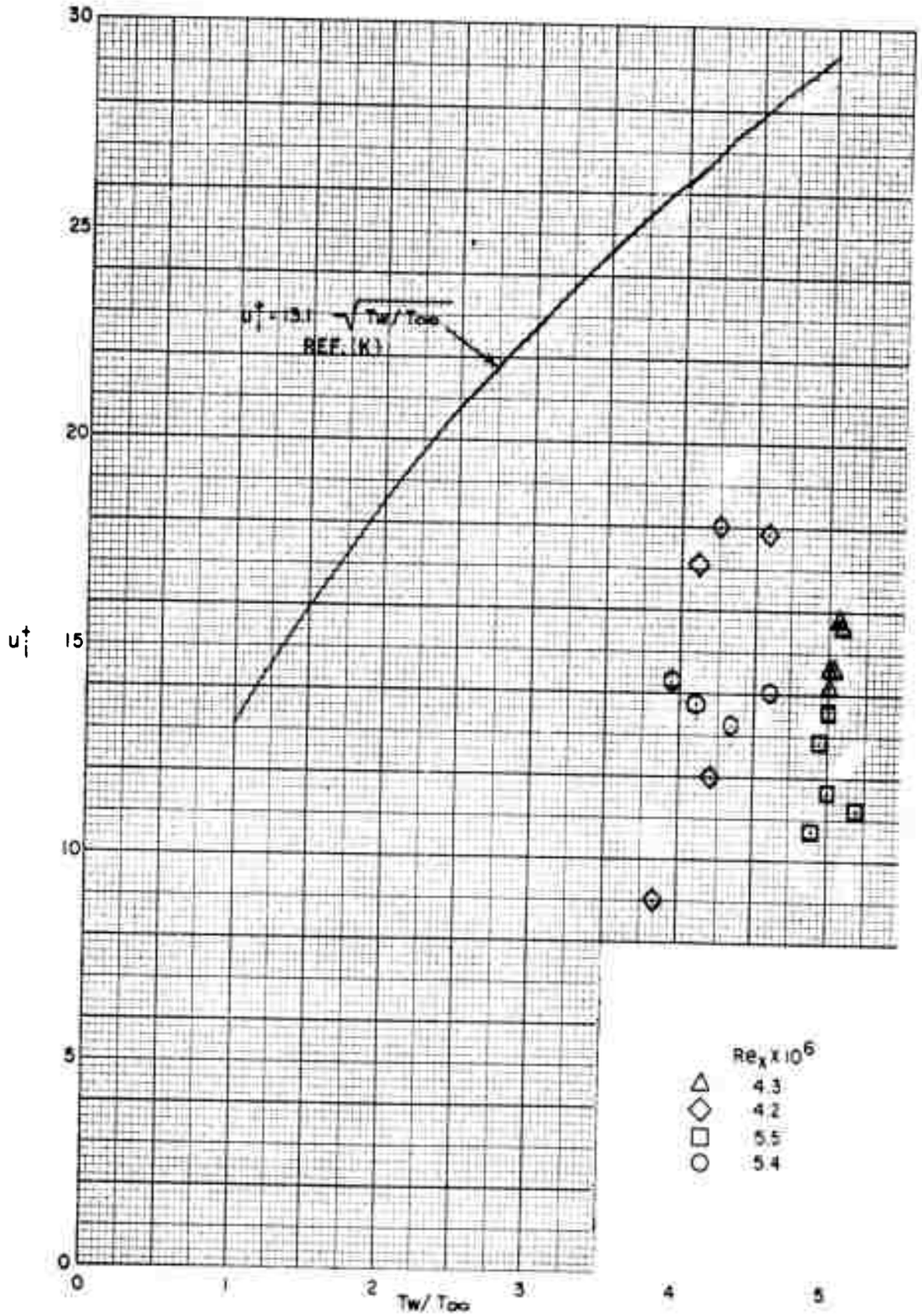

FIG. 22 INTERFACE NON-DIMENSIONAL VELOCITY, u_i^+, VERSUS T_w/T_∞

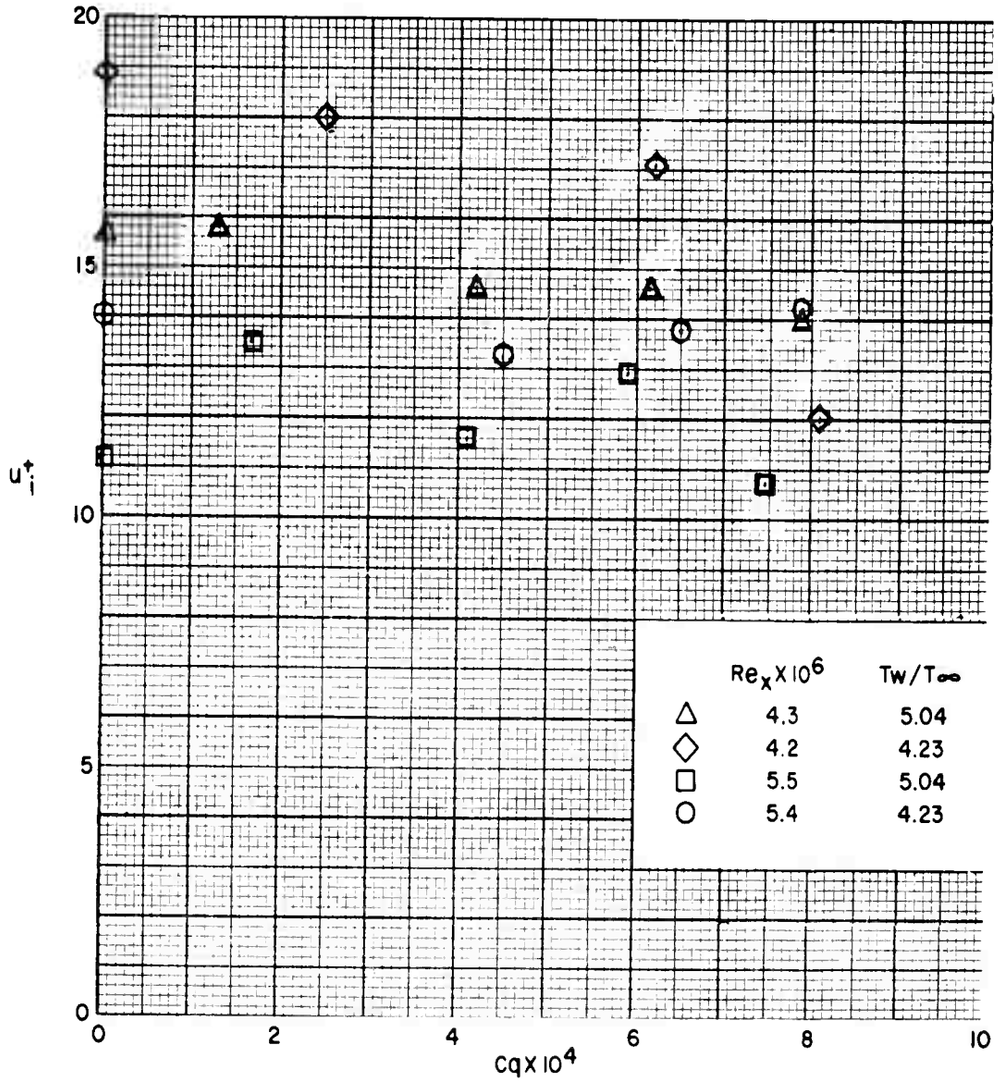

FIG. 23 INTERFACE NON-DIMENSIONAL VELOCITY, u_i^+, VERSUS INJECTION RATE Cq

TABLE I

$M_{\infty} = 5.05$		$P_o = 7.40$	atm
$Re_{\theta} = 3506$		$T_o = 376.5$	^oK
$C_q = 0$		$T_{\infty} = 61.71$	^oK
$(Te-Tw)/Te = 0.0847$		$U_{\infty} = 795.4$	m/sec
		$Tw/T_{\infty} = 5.085$	

Y (mm)	M	T/T_{∞}	U/U_{∞}
12.71	5.05	1.000	1.000
11.44	5.04	1.004	1.000
10.17	5.03	1.007	.999
8.903	5.03	1.007	.999
8.268	5.02	1.011	.999
7.633	5.02	1.011	.999
6.998	5.00	1.018	.999
6.363	4.97	1.026	.997
6.109	4.95	1.032	.996
5.728	4.90	1.047	.993
5.093	4.75	1.097	.985
4.458	4.52	1.182	.973
3.823	4.21	1.313	.955
3.188	3.89	1.469	.934
3.061	3.82	1.507	.928
2.553	3.55	1.667	.908
2.299	3.41	1.758	.895
2.048	3.29	1.843	.884
1.791	3.20	1.907	.875
1.537	3.10	1.985	.865
1.410	3.04	2.035	.859
1.283	2.94	2.122	.848
1.156	2.82	2.233	.834
1.029	2.68	2.373	.818
.902	2.52	2.545	.796
.775	2.34	2.753	.769
.648	2.13	3.014	.732
.597	2.05	3.122	.717
.521	1.80	3.462	.663
.470	1.69	3.617	.636
.394	1.44	3.986	.568
.343	1.26	4.231	.512
.292	1.07	4.476	.449

TABLE 2

$M_{\infty} = 5.06$		$P_o = 7.48$	atm
$Re_{\theta} = 3739$		$T_o = 378.2$	^oK
$C_q = 1.30 \times 10^{-4}$		$T_{\infty} = 61.56$	^oK
$(Te-Tw)/Te = 0.0911$		$U_{\infty} = 797.6$	m/sec
		$Tw/T_{\infty} = 5.070$	

Y (mm)	M	T/T_{∞}	U/U_{∞}
12.71	5.07	1.000	1.000
11.44	5.06	1.004	1.000
10.17	5.04	1.010	.999
9.538	5.03	1.014	.999
8.903	5.02	1.018	.999
8.268	5.03	1.014	.999
7.633	5.02	1.018	.999
6.998	5.00	1.024	.998
6.363	4.95	1.041	.996
5.728	4.83	1.080	.990
5.093	4.63	1.152	.980
4.458	4.37	1.255	.966
4.077	4.20	1.330	.955
3.823	4.06	1.398	.947
3.188	3.75	1.563	.925
2.553	3.42	1.770	.897
2.299	3.28	1.869	.885
2.045	3.19	1.935	.875
1.791	3.08	2.020	.863
1.537	2.97	2.109	.851
1.283	2.80	2.270	.831
1.156	2.69	2.376	.818
1.029	2.56	2.515	.801
.902	2.42	2.675	.781
.775	2.27	2.855	.757
.648	2.04	3.155	.715
.521	1.75	3.564	.652
.394	1.42	4.053	.564
.343	1.26	4.318	.516
.292	1.05	4.609	.445

TABLE 3

$M_\infty = 5.08$	$P_o = 7.67$ atm
$Re_\theta = 4523$	$T_o = 377.5$ °K
$C_q = 4.20 \times 10^{-4}$	$T_\infty = 61.27$ °K
$(Te-Tw)/Te = 0.0984$	$U_\infty = 797.2$ m/sec
	$Tw/T_\infty = 5.043$

Y (mm)	M	T/T_∞	U/U_∞
12.713	5.080	1.000	1.000
11.443	5.061	1.007	1.000
10.808	5.056	1.009	1.000
10.173	5.045	1.012	.999
9.538	5.033	1.017	.999
8.903	5.029	1.018	.999
8.268	5.015	1.022	.998
7.633	4.972	1.036	.996
6.998	4.911	1.056	.994
6.363	4.791	1.094	.987
5.728	4.576	1.173	.976
5.093	4.322	1.278	.962
4.458	4.028	1.418	.944
4.077	3.847	1.513	.932
3.823	3.738	1.574	.923
3.188	3.434	1.764	.898
2.553	3.132	1.979	.867
2.299	3.028	2.060	.856
2.045	2.932	2.140	.844
1.791	2.800	2.260	.829
1.537	2.669	2.388	.811
1.410	2.603	2.455	.803
1.283	2.503	2.563	.789
1.156	2.388	2.698	.772
1.029	2.295	2.809	.757
.902	2.168	2.966	.735
.775	2.017	3.166	.706
.648	1.829	3.425	.666
.521	1.611	3.737	.613
.394	1.289	4.204	.520
.343	1.122	4.434	.465
.292	1.005	4.586	.424

TABLE 4

M_{∞} = 5.09		P_o = 7.795	atm
Re_{θ} = 5108		T_o = 379.9	^oK
C_q = 6.16×10^{-4}		T_{∞} = 61.47	^oK
$(T_e - T_w)/T_e$ = 0.1064		U_{∞} = 800.12	m/sec
		T_w/T_{∞} = 5.013	

Y (mm)	M	T/T_{∞}	U/U_{∞}
12.71	5.09	1.000	1.000
11.44	5.06	1.010	.999
10.17	5.04	1.017	.999
9.538	5.03	1.020	.998
8.903	5.02	1.023	.998
8.268	4.96	1.043	.995
7.633	4.89	1.066	.992
6.998	4.78	1.103	.986
6.363	4.59	1.173	.977
5.728	4.32	1.285	.962
5.347	4.15	1.363	.952
5.093	4.05	1.410	.945
4.458	3.76	1.566	.924
3.823	3.48	1.735	.901
3.188	3.20	1.926	.874
3.061	3.16	1.966	.869
2.553	2.94	2.137	.844
2.299	2.82	2.249	.829
2.048	2.71	2.350	.816
1.791	2.58	2.482	.799
1.537	2.44	2.637	.778
1.283	2.28	2.827	.753
1.156	2.18	2.953	.736
1.029	2.06	3.110	.714
.902	1.96	3.246	.694
.775	1.82	3.440	.663
.648	1.67	3.646	.628
.521	1.46	3.947	.571
.470	1.39	4.051	.550
.394	1.18	4.341	.484
.343	1.08	4.471	.450
.292	.972	4.611	.410

TABLE 5

M_∞ = 5.09		P_o = 7.87		atm
Re_θ = 6178		T_o = 377.46		^oK
C_q = 7.89×10^{-4}		T_∞ = 61.07		^oK
$(Te-Tw)/Te$ = 0.1065		U_∞ = 797.6		m/sec
		Tw/T_∞ = 5.027		

Y (mm)	M	T/T_∞	U/U_∞
13.983	5.09	1.000	1.000
12.713	5.07	1.006	.999
11.443	5.05	1.013	.998
10.808	5.02	1.023	.998
10.173	5.01	1.026	.997
9.538	5.00	1.029	.997
8.903	4.94	1.048	.994
8.268	4.85	1.079	.990
7.633	4.74	1.117	.984
6.998	4.55	1.188	.974
6.617	4.42	1.243	.968
6.363	4.31	1.291	.962
5.728	4.01	1.431	.947
5.093	3.76	1.578	.926
4.458	3.52	1.718	.905
3.823	3.24	1.906	.879
3.188	2.97	2.120	.850
2.807	2.77	2.299	.825
2.553	2.69	2.374	.814
2.299	2.57	2.405	.798
2.045	2.43	2.644	.776
1.791	2.32	2.763	.758
1.537	2.18	2.934	.734
1.283	2.03	3.123	.705
1.156	1.96	3.215	.690
1.036	1.89	3.310	.676
1.029	1.87	3.341	.672
.902	1.79	3.451	.653
.826	1.72	3.547	.636
.775	1.66	3.633	.622
.648	1.54	3.807	.590
.572	1.45	3.940	.565
.521	1.40	4.014	.551
.470	1.29	4.166	.517
.394	1.15	4.363	.472
.292	.93	4.640	.394

TABLE 6

M_∞ = 5.09		P_o = 7.50	atm
Re_θ = 3186		T_o = 369.3	^oK
C_q = 0		T_∞ = 59.83	^oK
$(T_e-T_w)/T_e$ = 0.183		U_∞ = 788.8	m/sec
		T_w/T_∞ = 4.595	

Y (mm)	M	T/T_∞	U/U_∞
8.727	5.086	1.000	1.000
6.187	5.051	1.012	.999
5.552	4.968	1.038	.995
4.917	4.796	1.095	.987
4.282	4.528	1.196	.974
3.647	4.245	1.318	.958
3.266	4.057	1.407	.946
3.012	3.928	1.474	.938
2.758	3.796	1.547	.928
2.504	3.651	1.632	.917
2.377	3.561	1.695	.912
2.250	3.530	1.713	.908
2.123	3.415	1.787	.898
1.996	3.376	1.813	.894
1.869	3.331	1.845	.890
1.742	3.302	1.866	.887
1.615	3.277	1.885	.885
1.488	3.265	1.894	.883
1.361	3.204	1.944	.878
1.234	3.143	1.995	.873
1.107	2.946	2.170	.853
.980	2.787	2.323	.835
.853	2.679	2.436	.822
.726	2.478	2.658	.794
.599	2.233	2.957	.755
.472	1.922	3.377	.694
.396	1.720	3.667	.648
.345	1.512	3.974	.593
.320	1.320	4.257	.535
.295	1.310	4.267	.532

TABLE 7

M_∞ = 5.05		P_o = 7.26	atm
Re_θ = 3915		T_o = 372.62	°K
Cq = 2.52×10^{-4}		T_∞ = 61.07	°K
(Te-Tw)/Te = 0.236		U_∞ = 791.29	m/sec
		T_w/T_∞ = 4.257	

Y (mm)	M	T/T_∞	U/U_∞
7.991	5.049	1.000	1.000
7.356	5.027	1.008	1.000
6.721	4.955	1.033	.997
6.086	4.866	1.084	.991
5.451	4.572	1.170	.979
4.816	4.300	1.281	.964
4.181	4.003	1.422	.945
3.927	3.891	1.481	.938
3.673	3.779	1.542	.929
3.419	3.652	1.616	.919
3.165	3.525	1.695	.909
2.911	3.354	1.812	.894
2.657	3.260	1.879	.885
2.403	3.147	1.964	.873
2.149	3.030	2.056	.860
1.895	2.945	2.126	.850
1.641	2.850	2.208	.839
1.463	2.690	2.364	.819
1.387	2.716	2.388	.822
1.260	2.640	2.414	.812
1.133	2.534	2.528	.798
1.006	2.428	2.647	.782
.955	2.315	2.782	.765
.879	2.310	2.786	.764
.752	2.082	3.076	.723
.701	2.016	3.165	.710
.625	2.000	3.186	.707
.574	1.840	3.406	.672
.523	1.802	3.460	.664
.473	1.658	3.666	.629
.396	1.344	4.123	.540
.345	1.204	4.322	.496
.320	1.147	4.401	.476
.295	1.072	4.504	.450

TABLE 8

M_∞	4.94	P_o	6.64	atm
Re_θ	4747	T_o	375.32	^oK
C_q	6.18×10^{-4}	T_∞	63.92	^oK
(Te-Tw)/Te	0.235	U_∞	791.39	m/sec
		T_w/T_∞	4.107	

Y (mm)	M	T/T_∞	U/U_∞
9.423	4.937	1.000	1.000
9.042	4.927	1.003	1.000
8.788	4.910	1.008	.999
8.534	4.910	1.008	.999
8.153	4.862	1.024	.997
7.772	4.838	1.032	.995
7.518	4.787	1.050	.994
6.883	4.654	1.096	.987
6.248	4.430	1.182	.976
5.613	4.196	1.280	.962
4.978	3.942	1.399	.944
4.343	3.707	1.521	.926
3.708	3.440	1.676	.902
3.073	3.199	1.830	.877
2.438	2.944	2.018	.847
2.184	2.848	2.093	.835
1.930	2.759	2.165	.822
1.676	2.640	2.269	.806
1.549	2.566	2.340	.795
1.422	2.484	2.419	.783
1.295	2.392	2.514	.768
1.168	2.284	2.635	.751
1.041	2.185	2.751	.734
.914	2.070	2.891	.713
.864	2.017	2.956	.702
.787	1.935	3.060	.686
.711	1.840	3.182	.665
.660	1.768	3.275	.648
.610	1.721	3.338	.637
.533	1.547	3.572	.592
.406	1.222	4.003	.495
.330	1.096	4.151	.453
.292	1.027	4.229	.428

TABLE 9

M_∞	4.98	P_o	7.09	atm
Re_θ	6092	T_o	370.55	°K
C_q	8.10×10^{-4}	T_∞	62.22	°K
$(T_e-T_w)/T_e$	0.225	U_∞	787.28	m/sec
		T_w/T_∞	4.219	

Y (mm)	M	T/T_∞	U/U_∞
10.84	4.978	1.000	1.000
10.20	4.971	1.002	1.000
9.566	4.952	1.009	.999
9.058	4.876	1.035	.997
8.804	4.846	1.046	.996
8.296	4.717	1.092	.990
7.788	4.657	1.113	.987
7.534	4.531	1.158	.980
7.280	4.356	1.232	.971
7.026	4.230	1.288	.964
6.772	4.163	1.317	.960
6.264	3.951	1.420	.946
5.756	3.716	1.548	.929
5.248	3.483	1.690	.910
4.740	3.250	1.850	.888
4.232	3.044	2.005	.866
3.724	2.845	2.170	.842
3.216	2.624	2.372	.812
2.962	2.542	2.450	.799
2.708	2.428	2.566	.781
2.454	2.349	2.646	.768
2.200	2.216	2.794	.744
1.946	2.107	2.918	.723
1.692	2.004	3.040	.702
1.438	1.882	3.190	.675
1.184	1.777	3.328	.651
.930	1.600	3.568	.607
.676	1.446	3.782	.565
.599	1.410	3.830	.554
.523	1.389	3.857	.548
.422	1.325	3.942	.528
.396	1.297	3.978	.520
.371	1.222	4.081	.496
.345	1.196	4.113	.487
.295	1.047	4.301	.436

TABLE 10

M_∞ =	4.85	P_o =	7.07	atm
Re_θ =	10,931	T_o =	375.32	^oK
C_q =	17.8×10^{-4}	T_∞ =	65.79	^oK
$(T_e-T_w)/T_e$ =	0.263	U_∞ =	788.73	m/sec
		T_w/T_∞ =	3.845	

Y (mm)	M	T/T_∞	U/U_∞
14.62	4.850	1.000	1.000
13.35	4.710	1.054	.997
12.84	4.626	1.084	.993
12.33	4.480	1.140	.986
11.83	4.268	1.227	.975
11.32	4.090	1.305	.963
10.81	3.815	1.442	.945
10.30	3.638	1.534	.929
9.794	3.510	1.601	.916
9.286	3.193	1.812	.886
8.753	2.926	2.011	.856
8.270	2.822	2.084	.840
7.762	2.590	2.288	.808
7.254	2.393	2.476	.776
6.746	2.270	2.605	.755
6.238	2.079	2.806	.718
5.730	1.966	2.927	.693
5.222	1.805	3.112	.657
4.714	1.682	3.250	.625
4.206	1.519	3.440	.581
3.444	1.366	3.597	.534
3.190	1.283	3.689	.508
2.682	1.124	3.856	.455
2.174	1.060	3.898	.432
1.666	.992	3.943	.406
1.158	.844	4.070	.351
.650	.707	4.176	.298
.396	.562	4.289	.240
.371	.552	4.297	.236
.345	.543	4.300	.232
.320	.514	4.319	.220
.295	.493	4.333	.212

TABLE II

M_{oo} = 5.18		P_o = 9.646	atm
Re_θ = 4000		T_o = 379.0	^oK
Cq = 0		T_∞ = 59.57	^oK
(Te-Tw)/Te = 0.0995		U_∞ = 801.6	m/sec
		Tw/T_∞ = 5.21	

Y (mm)	M	T/T_∞	U/U_∞
9.373	5.18	1.000	1.000
8.738	5.18	1.000	1.000
8.103	5.17	1.004	1.000
7.468	5.13	1.018	.999
6.833	5.05	1.044	.996
6.198	4.89	1.103	.991
5.563	4.67	1.188	.983
4.928	4.40	1.306	.971
4.293	4.11	1.444	.954
3.658	3.82	1.599	.932
3.023	3.51	1.793	.907
2.515	3.27	1.953	.882
2.261	3.16	2.034	.870
2.007	3.04	2.127	.856
1.753	2.94	2.213	.844
1.499	2.85	2.294	.833
1.245	2.77	2.367	.823
.991	2.62	2.527	.804
.864	2.51	2.649	.789
.737	2.39	2.789	.771
.610	2.24	2.974	.746
.483	2.04	3.243	.709
.432	1.94	3.345	.685
.381	1.82	3.500	.659
.330	1.67	3.710	.623
.279	1.55	3.850	.589
.229	1.42	4.030	.553
.203	1.29	4.200	.513
.178	1.19	4.350	.480

TABLE 12

$M_\infty = 5.14$		$P_o = 8.05$	atm
$Re_\theta = 4500$		$T_o = 380.5$	^oK
$Cq = 1.69 \times 10^{-4}$		$T_\infty = 60.54$	^oK
$(Te-Tw)/Te = 0.1167$		$U_\infty = 801.9$	m/sec
		$Tw/T_\infty = 5.038$	

Y (mm)	M	T/T_∞	U/U_∞
10.64	5.14	1.000	1.000
9.373	5.14	1.000	1.000
8.738	5.12	1.007	1.000
8.103	5.09	1.018	.999
6.833	4.87	1.095	.992
6.198	4.68	1.169	.984
5.563	4.43	1.277	.974
4.928	4.15	1.408	.958
4.293	3.87	1.554	.939
3.658	3.58	1.725	.915
3.023	3.31	1.898	.887
2.388	3.02	2.119	.855
1.753	2.79	2.311	.825
1.499	2.70	2.393	.813
1.245	2.60	2.491	.798
.991	2.46	2.637	.777
.864	2.37	2.742	.763
.737	2.24	2.900	.743
.610	2.11	3.050	.717
.483	1.92	3.298	.678
.432	1.81	3.448	.654
.381	1.72	3.573	.632
.330	1.61	3.725	.604
.279	1.47	3.914	.566
.229	1.33	4.144	.515
.203	1.19	4.278	.479
.152	1.06	4.415	.431

TABLE 13

M_{oo} = 5.14		P_o = 9.98	atm
Re_θ = 5590		T_o = 380.0	^oK
Cq = 4.24×10^{-4}		T_∞ = 60.48	^oK
(Te-Tw)/Te = 0.1135		U_∞ = 801.48	m/sec
		Tw/T_∞ = 5.08	

Y (mm)	M	T/T_∞	U/U_∞
11.28	5.14	1.000	1.000
10.64	5.14	1.000	1.000
10.01	5.12	1.007	1.000
9.373	5.07	1.025	.999
8.738	4.97	1.062	.996
8.103	4.82	1.119	.992
7.468	4.63	1.196	.985
6.833	4.41	1.289	.974
6.198	4.175	1.399	.961
5.563	3.93	1.525	.944
4.928	3.66	1.685	.924
4.293	3.42	1.835	.901
3.658	3.165	2.015	.874
3.023	2.935	2.195	.846
2.388	2.71	2.390	.815
1.753	2.48	2.613	.780
1.499	2.39	2.711	.766
1.245	2.28	2.839	.747
.991	2.14	3.019	.723
.864	2.03	3.167	.703
.737	1.93	3.267	.679
.610	1.80	3.437	.649
.483	1.62	3.690	.605
.432	1.54	3.801	.584
.381	1.44	3.942	.556
.330	1.34	4.085	.527
.279	1.23	4.234	.492
.254	1.17	4.315	.473
.229	1.10	4.406	.449
.203	1.02	4.510	.421
.165	.905	4.638	.379
.152	.860	4.684	.362

TABLE 14

M_∞ = 5.07		P_o = 10.10	atm
Re_θ = 6100		T_o = 379.0	^oK
Cq = 6.18×10^{-4}		T_∞ = 61.70	^oK
(Te-Tw)/Te = 0.115		U_∞ = 798.5	m/sec
		T_w/T_∞ = 4.935	

Y (mm)	M	T/T_∞	U/U_∞
10.617	5.07	1.000	1.000
9.982	5.01	1.024	1.000
9.347	4.87	1.077	.997
8.712	4.70	1.144	.992
8.077	4.50	1.227	.983
7.442	4.28	1.324	.971
6.807	4.05	1.436	.957
6.172	3.807	1.570	.941
5.537	3.57	1.712	.921
4.902	3.33	1.862	.896
4.267	3.09	2.037	.870
3.632	2.887	2.202	.845
2.997	2.67	2.371	.811
2.362	2.46	2.572	.778
1.981	2.30	2.740	.751
1.727	2.23	2.816	.738
1.473	2.11	2.956	.716
1.219	2.00	3.080	.692
.965	1.88	3.241	.667
.711	1.71	3.463	.628
.584	1.58	3.638	.594
.457	1.45	3.815	.559
.330	1.26	4.069	.501
.203	1.03	4.346	.424
.152	.867	4.527	.364

TABLE 15

M_∞	5.10	P_o	10.28	atm
Re_θ	7689	T_o	379.3	^oK
C_q	7.46×10^{-4}	T_∞	61.18	^oK
(Te-Tw)/Te	0.129	U_∞	799.7	m/sec
		T_w/T_∞	4.904	

Y (mm)	M	T/T_∞	U/U_∞
13.18	5.099	1.000	1.000
10.64	4.914	1.066	.995
8.103	4.120	1.406	.958
6.833	3.619	1.690	.923
5.563	3.204	1.955	.878
5.309	3.119	2.010	.867
5.055	3.044	2.072	.859
4.801	2.957	2.139	.848
4.547	2.875	2.205	.837
4.293	2.801	2.274	.828
4.039	2.704	2.349	.813
3.785	2.644	2.400	.803
3.531	2.559	2.479	.790
3.277	2.476	2.559	.777
3.023	2.386	2.648	.761
2.896	2.329	2.708	.752
2.769	2.292	2.746	.745
2.642	2.252	2.788	.737
2.515	2.209	2.833	.729
2.261	2.162	2.880	.720
2.007	2.036	3.030	.695
1.753	1.944	3.189	.681
1.499	1.850	3.255	.655
1.245	1.742	3.395	.629
.991	1.611	3.566	.597
.737	1.464	3.768	.557
.483	1.235	4.080	.489
.356	1.032	4.346	.422
.229	.874	4.529	.365
.152	.770	4.626	.325

TABLE 16

M_∞ = 5.20		P_o = 8.39	atm
Re_θ = 4011		T_o = 383.14	^oK
C_q = 0		T_∞ = 59.81	^oK
$(T_e-T_w/T_e$ = 0.210		U_∞ = 806.4	m/sec
		T_w/T_∞ = 4.615	

Y (mm)	M	T/T_∞	U/U_∞
8.230	5.20	1.000	1.000
7.722	5.19	1.004	1.000
7.214	5.15	1.017	.999
6.960	5.12	1.028	.998
6.325	4.99	1.074	.994
5.944	4.89	1.109	.990
5.690	4.80	1.144	.987
5.055	4.54	1.246	.975
4.928	4.48	1.276	.972
4.420	4.27	1.367	.960
3.785	3.96	1.523	.939
3.150	3.67	1.687	.915
2.388	3.38	1.864	.886
2.134	3.18	2.013	.866
1.880	3.08	2.086	.854
1.372	2.90	2.217	.829
1.118	2.80	2.297	.815
1.067	2.75	2.343	.809
.991	2.69	2.398	.801
.914	2.64	2.445	.794
.864	2.60	2.480	.787
.737	2.47	2.614	.768
.610	2.30	2.810	.741
.483	2.08	3.074	.701
.356	1.75	3.510	.631
.305	1.56	3.744	.589
.254	1.42	3.975	.544
.203	1.27	4.183	.498
.178	1.12	4.380	.451
.152	.999	4.524	.409

TABLE 17

M_{∞} =	5.16	P_o =	8.283	atm
Re_{θ} =	5786	T_o =	387.55	°K
C_q =	4.53×10^{-4}	T_{∞} =	61.27	°K
$(T_e - T_w)/T_e$ =	0.2428	U_{∞} =	809.9	m/sec
		T_w/T_{∞} =	4.363	

Y (mm)	M	T/T_{∞}	U/U_{∞}
10.744	5.16	1.000	1.000
9.474	5.09	1.024	.998
8.839	5.01	1.053	.996
8.204	4.88	1.100	.992
7.569	4.69	1.173	.984
6.934	4.49	1.257	.976
6.680	4.38	1.305	.970
6.299	4.26	1.363	.964
5.664	4.03	1.474	.948
5.029	3.77	1.612	.928
4.394	3.52	1.759	.903
3.759	3.28	1.906	.878
3.124	3.05	2.066	.850
2.489	2.82	2.238	.818
1.854	2.60	2.421	.784
1.219	2.33	2.671	.738
1.092	2.25	2.754	.724
.838	2.09	2.928	.693
.584	1.85	3.213	.644
.457	1.69	3.436	.605
.330	1.46	3.736	.547
.279	1.34	3.890	.512
.229	1.19	4.078	.464
.178	1.072	4.200	.426
.152	.956	4.328	.385

TABLE 18

M_∞ = 5.12		P_o = 7.926	atm
Re_θ = 6736		T_o = 381.65	^oK
Cq = 6.53×10^{-4}		T_∞ = 61.64	^oK
(Te-Tw)/Te = 0.2793		U_∞ = 802.7	m/sec
		Tw/T_∞ = 4.105	

Y (mm)	M	T/T_∞	U/U_∞
10.719	5.12	1.000	1.000
9.957	5.01	1.036	.996
9.449	4.91	1.074	.994
8.941	4.76	1.131	.989
8.179	4.52	1.230	.979
7.544	4.296	1.331	.968
6.909	4.08	1.435	.955
6.274	3.86	1.551	.939
5.639	3.61	1.694	.918
5.004	3.38	1.835	.894
4.369	3.158	1.985	.869
3.734	2.946	2.132	.840
3.099	2.745	2.280	.810
2.464	2.540	2.445	.776
1.829	2.300	2.655	.732
1.575	2.200	2.750	.713
1.321	2.086	2.866	.690
1.067	1.968	2.990	.665
.813	1.818	3.158	.631
.559	1.602	3.419	.579
.432	1.436	3.629	.534
.305	1.232	3.886	.474
.152	.897	4.272	.362

TABLE 19

M_∞ = 5.03		P_o = 7.346	atm
Re_θ = 7475		T_o = 382.77	°K
C_q = 7.88×10^{-4}		T_∞ = 63.18	°K
$(T_e - T_w)/T_e$ = 0.2825		U_∞ = 801.6	m/sec
		T_w/T_∞ = 3.973	

Y (mm)	M	T/T_∞	U/U_∞
11.176	5.02	1.000	1.000
9.906	4.76	1.098	.991
8.636	4.25	1.323	.972
7.366	4.19	1.325	.959
6.096	3.50	1.700	.907
4.826	3.37	1.737	.883
4.191	2.86	2.118	.827
3.556	2.59	2.337	.787
2.921	2.41	2.478	.754
2.286	2.15	2.720	.705
2.032	2.07	2.792	.688
1.778	1.96	2.902	.664
1.524	1.86	3.000	.640
1.270	1.80	3.057	.626
1.016	1.66	3.209	.591
.762	1.57	3.293	.566
.635	1.48	3.391	.543
.508	1.44	3.430	.530
.381	1.34	3.540	.501
.254	1.25	3.041	.474
.229	1.196	3.703	.458
.178	1.114	3.793	.431
.152	1.072	3.838	.418

TABLE 20
SUMMARY OF BOUNDARY-LAYER PARAMETERS

M_∞	T_w/T_∞	C_q	δ	δ^*	θ	n	Re_θ	Re_x	C_f
					Set 1 - 29.25 cm Station				
5.05	5.085	0	6.1	2.52	0.242	9.1	3506	4.22×10^6	9.36×10^{-4}
5.06	5.070	1.30×10^{-4}	6.4	2.75	0.257	8.3	3739	4.26×10^6	8.36×10^{-4}
5.08	5.043	4.20×10^{-4}	7.2	3.30	0.307	7.1	4523	4.31×10^6	7.60×10^{-4}
5.09	5.010	6.16×10^{-4}	7.7	3.76	0.347	6.1	5108	4.31×10^6	6.80×10^{-4}
5.09	5.027	7.88×10^{-4}	8.2	4.30	0.410	5.2	6178	4.41×10^6	6.06×10^{-4}
					Set 2 - 29.25 cm Station				
5.09	4.595	0	6.0	2.33	0.214	9.5	3186	4.35×10^6	7.83×10^{-4}
5.05	4.257	2.52×10^{-4}	6.7	2.99	0.272	7.5	3915	4.13×10^6	7.12×10^{-4}
4.94	4.107	6.18×10^{-4}	7.6	3.47	0.347	6.7	4747	4.00×10^6	6.55×10^{-4}
4.98	4.219	9.10×10^{-4}	8.3	4.57	0.419	4.4	6092	4.25×10^6	6.45×10^{-4}
4.85	3.845	17.80×10^{-4}	12.5	8.53	0.722	2.1	10931	4.05×10^6	2.05×10^{-4}
					Set 3 - 36.85 cm Station				
5.18	5.204	0	6.9	3.05	0.265	8.5	4000	5.56×10^6	12.90×10^{-4}
5.14	5.038	1.69×10^{-4}	7.2	3.39	0.300	7.7	4500	5.51×10^6	9.21×10^{-4}
5.14	5.079	4.12×10^{-4}	8.4	4.30	0.367	6.3	5590	5.61×10^6	9.49×10^{-4}
5.07	4.935	5.92×10^{-4}	9.0	4.85	0.418	5.3	6100	5.37×10^6	7.29×10^{-4}
5.10	4.904	7.46×10^{-4}	9.7	5.78	0.507	4.2	7689	5.59×10^6	6.63×10^{-4}
					Set 4 - 36.85 cm Station				
5.20	4.615	0	6.8	2.94	0.268	8.6	4011	5.51×10^6	10.68×10^{-4}
5.16	4.363	4.53×10^{-4}	8.7	4.16	0.393	6.3	5786	5.42×10^6	8.59×10^{-4}
5.12	4.105	6.53×10^{-4}	9.0	4.87	0.457	5.6	6736	5.44×10^6	6.91×10^{-4}
5.03	3.973	7.88×10^{-4}	9.5	5.39	0.532	3.9	7475	5.18×10^6	5.61×10^{-4}

AERODYNAMICS DEPARTMENT
EXTERNAL DISTRIBUTION LIST (A1)

No. of Copies	
	Chief, Bureau of Naval Weapons Department of the Navy Washington 25, D. C.
1	Attn: DLI-30
1	Attn: R-14
1	Attn: RRRE-7
1	Attn: RMMS-53
	Office of Naval Research Room 2709, T-3 Washington 25, D. C.
1	Attn: Head, Mechanics Br.
	Director, DTMB Aerodynamics Laboratory Washington 7, D. C.
1	Attn: Library
	Officer in Charge, NPG Dahlgren, Virginia
1	Attn: Library
	Commander, U. S. NOTS China Lake, California
1	Attn: Technical Library
1	Attn: Code 503
1	Attn: Code 406
	Director, NRL Washington 25, D. C.
1	Attn: Code 2027
1	Commanding Officer Office of Naval Research Branch Office Box 39, Navy 100 Fleet Post Office New York, N. Y.
	NASA High Speed Flight Station Box 273 Edwards Air Force Base, California
1	Attn: W. C. Williams
	NASA Ames Aeronautical Laboratory Moffett Field, California
1	Attn: Librarian

No. of Copies	
	NASA Langley Aeronautical Laboratory Langley Field, Virginia
3	Attn: Librarian
1	Attn: C. H. McLellan
1	Attn: J. J. Stack
1	Attn: Adolf Busemann
1	Attn: Comp. Res. Div.
1	Attn: Theoretical Aerodynamics Div.
	NASA Lewis Flight Propulsion Lab. 21000 Brookpark Road Cleveland 11, Ohio
1	Attn: Librarian
1	Attn: Chief, Propulsion Aerodynamics Div.
	NASA 1520 H Street, N. W. Washington 25, D. C.
1	Attn: Chief, Division of Research Information
	Office of the Assistant Secretary of Defense (R & D) Room 3E1065, The Pentagon Washington 25, D. C.
1	Attn: Technical Library
	Research and Development Board Room 3D1041, The Pentagon Washington 25, D. C.
2	Attn: Library
10	ASTIA Arlington Hall Station Arlington 12, Virginia Attn: TIPDR
	Commander, NAMTC Point Mugu, California
1	Attn: Technical Library
	Commanding General Aberdeen Proving Ground, Md.
1	Attn: Technical Info. Br.
1	Attn: Ballistics Res. Lab.

AERODYNAMICS DEPARTMENT
EXTERNAL DISTRIBUTION LIST (A1)

No. of Copies	
	Director, Special Projects Department of the Navy Washington 25, D. C.
1	Attn: SP-2722
	Director of Intelligence Headquarters, USAF Washington 25, D. C.
1	Attn: AFOIN-3B
	Commander, WADC Wright-Patterson AF Base Ohio
2	Attn: WCOSI-3
1	Attn: WCLSW-5
3	Attn: WCRRD
	ARDC Regional Office Room 4549 Munitions Bldg. c/o Dept. of the Navy Washington 25, D. C.
1	Attn: Maj. T. J. Borgstrom
	Air Force Ballistic Missile Div. HQ Air Research & Development Command P. O. Box 262 Inglewood, California
1	Attn: WDTLAR
	Chief, AFSWP Washington 25, D. C.
1	Attn: Document Library
	Commanding General Arnold Engineering Development Center Tullahoma, Tennessee
1	Attn: Technical Library
5	Attn: AEKS
	Commanding Officer, DOFL Washington 25, D. C.
1	Attn: Library Room 211, Bldg. 92

No. of Copies	
	Commanding General Army Ballistic Missile Agency Huntsville, Alabama
1	Attn: ORDAB-DA
1	Attn: Dr. E. Geissler
1	Attn: Mr. T. Reed
1	Attn: Mr. H. Paul
1	Attn: Mr. W. Dahm
	Commanding General Redstone Arsenal Huntsville, Alabama
1	Attn: Mr. N. Shapiro ORDDW-MRF
	Office, Chief Of Ordnance Department of the Army Washington 25, D. C.
1	Attn: ORDTU
	APL/JHU (C/NOw 7386) 8621 Georgia Avenue Silver Spring, Maryland
2	Attn: Tech. Reports Group
1	Attn: Mr. D. Fox
1	Attn: Dr. F. Hill
	Via: INSORD

AERODYNAMICS DEPARTMENT
EXTERNAL DISTRIBUTION LIST (A2)

No. of Copies		No. of Copies	
	Superintendent U. S. Naval Postgraduate School Monterey, California		General Applied Science Laboratories, Inc. Merrick and Stewart Avenues Westbury, L. I., New York
1	Attn: Tech. Rpts. Section Library	1 1	Attn: Mr. Walter Daskin Attn: Mr. R. W. Byrne
	National Bureau of Standards Washington 25, D. C.	1	CONVAIR A Division of Feneral Dynamics Corporation Fort Worth, Texas
1	Attn: Chief, Fluid Mechanics Section		
	University of Minnesota Rosemount Research Laboratories Rosemount, Minnesota		United Aircraft Corporation 400 Main Street East Hartford 8, Connecticut
1	Attn: Technical Library	1 2	Attn: Chief Librarian Attn: Mr. W. Kuhrt, Research Dept.
1	Director Air University Library Maxwell AF Base, Alabama	1	Attn: Mr. J. G. Lee
	Douglas Aircraft Company, Inc. Santa Monica Division 3000 Ocean Park Boulevard Santa Monica, California	1	Hughes Aircraft Company Florence Avenue at Teale St. Culver City, California Attn: Mr. D. H. Johnson R & D Tech. Library
1	Attn: Chief Missiles Engineer		
1	Attn: Aerodynamics Section	1	McDonnell Aircraft Corporation P. O. Box 516 St. Louis 3, Missouri
1	CONVAIR A Division of General Dynamics Corporation Daingerfield, Texas		
	CONVAIR	1	Lockheed Aircraft Corporation Lockheed Missiles and Space Div. Sunnyvale, California Attn: Dr. L. H. Wilson
	Scientific Research Laboratory	4	Attn: Mr. W. E. Brandt
	5001 Kearney Villa Road	1	Attn: Mr. M. Tucker
	San Diego 11, California	1	Attn: Mr. B. W. March
1	Attn: Mr. M. Sibulkin	1	Attn: Mr. W. J. Fleming, Jr.
1	Attn: Asst. to the Dir. of Scientific Research		
	Republic Aviation Corporation Farmingdale, New York	1 1	The Martin Company Baltimore 3, Maryland Attn: Library Attn: Chief Aerodynamicist
1	Attn: Technical Library		
			North American Aviation, Inc. Aerophysics Laboratory Downing, California
		1	Attn: Dr. E. R. Van Driest

AERODYNAMICS DEPARTMENT
EXTERNAL DISTRIBUTION LIST (A2)

No. of Copies	
	Case Institute of Technology Cleveland 6, Ohio
1	Attn: G. Kuerti
1	Mr. J. Lukasiewicz Chief, Gas Dynamics Facility ARO, Incorporated Tullahoma, Tennessee
	Massachusetts Institute of Technology Cambridge 39, Massachusetts
1	Attn: Prof. J. Kaye
1	Attn: Prof. M. Finston
1	Attn: Mr. J. Baron
1	Attn: Mr. M. Sweeney, Jr.
	New York University 45 Fourth Avenue New York 3, New York
1	Attn: Prof. R. Courant
1	Attn: Prof. H. Ludloff
	Polytechnic Institute of Brooklyn 527 Atlantic Avenue Freeport, New York
1	Attn: Dr. A. Ferri
1	Attn: Dr. M. Bloom
1	Attn: Dr. P. Libby
	Brown University Division of Engineering Providence, Rhode Island
1	Attn: Prof. R. Probstein
1	Attn: Prof. C. Lin
	University of Minnesota Minneapolis 14, Minnesota
1	Attn: Dr. E. R. G. Eckert
1	Attn: Dr. J. Hartnett
1	Attn: Heat Transfer Lab.
1	Attn: Tech. Library
	Rensselaer Polytechnic Institute Troy, New York
1	Attn: Dept. of Aeronautical Engineering

No. of Copies	
	Princeton University James Forrestal Research Center Gas Dynamics Laboratory Princeton, New Jersey
1	Attn: Prof. S. Bogdonoff
	Institute for Fluid Dynamics and Applied Mathematics University of Maryland College Park, Maryland
2	Attn: Director
1	Attn: Dr. J. Burgers
	University of Michigan Ann Arbor, Michigan
1	Attn: Dr. A. Kuethe
1	Applied Mathematics and Statistics Laboratory Stanford University Stanford, California
	Cornell University Graduate School of Aero. Engr. Ithaca, New York
1	Attn: Prof. W. R. Sears
	The Johns Hopkins University Charles and 34th Streets Baltimore, Maryland
1	Attn: Dr. F. H. Clauser
	University of California Berkeley 4, California
1	Attn: G. Maslach
1	Attn: Dr. S. Schaaf
1	Air Ballistics Laboratory Army Ballistic Missile Agency Huntsville, Alabama
1	Mr. Rex Monaghan RAE, Farnsborough, England c/o British Joint Services Mission Attn: Aircraft Branch P. O. Box 680 Benjamin Franklin Stations Washington, D. C.

AERODYNAMICS DEPARTMENT
EXTERNAL DISTRIBUTION LIST (A2)

No. of Copies	
1	BuWeps Representative Aerojet-General Corporation 6352 N. Irwindale Avenue Azusa, California
1	Boeing Airplane Company Seattle, Washington
	RAND Corporation 1700 Main Street Santa Monica, California
1	Attn: Lib., USAF Project RAND
	Arnold Research Organization, Inc. Tullahoma, Tennessee
1	Attn: Tech. Library
1	Attn: Chief, Propulsion Wind Tunnel
1	Attn: Dr. J. L. Potter
	General Electric Company Missile and Space Vehicle Dept. 3198 Chestnut Street Philadelphia, Pennsylvania
2	Attn: Larry Chasen Mgr. Library
1	Attn: Mr. R. Kirby
1	Attn: Dr. J. Farber
1	Attn: Dr. G. Sutton
1	Attn: Dr. J. D. Stewart
1	Attn: Dr. S. M. Scala
1	Attn: Dr. H. Lew
	Eastman Kodak Company Navy Ordnance Division 50 West Main Street Rochester 14, New York
2	Attn: W. B. Forman
	Reports Distribution Office AVCO-EVERETT Research Lab. 2385 Revere Beach Parkway Everett 49, Massachusetts
3	Attn: Dr. J. Ekerman

No. of Copies	
1	AER, Incorporated 871 East Washington Street Pasadena, California
	Armour Research Foundation 10 West 35th Street Chicago 16, Illinois
2	Attn: Dept. M
	Chance-Vought Aircraft, Inc. Dallas, Texas
2	Attn: Librarian
	Ramo-Woolridge Corporation Guided Missiles Research Div. Los Angeles 45, California
1	Attn: Dr. G. Solomon
	Cornell Aeronautical Lab., Inc. 4455 Genesee Street Buffalo 21, New York
1	Attn: Librarian
1	Attn: Dr. Franklin Moore
	Defense Research Laboratory The University of Texas P. O. Box 8029 Austin 12, Texas
1	Attn: Assistant Director
	Ohio State University Columbus 10, Ohio
1	Attn: Security Officer
1	Attn: Aerodynamics Lab.
1	Attn: Mr. J. Lee
1	Attn: Chairman, Dept. of Aeronautical Engin'ing
	CIT Pasadena, California
1	Attn: Guggenheim Aeronautical Lab., Aeronautics Library
1	Attn: Jet Propulsion Lab.
1	Attn: Dr. H. Liepmann
1	Attn: Dr. L. Lees
1	Attn: Dr. D. Coles
1	Attn: Mr. A. Roshko
1	Attn: Mr. S. Dhawan

AERODYNAMICS DEPARTMENT
EXTERNAL DISTRIBUTION LIST (A2)

No. of Copies	
1	Applied Mechanics Reviews Southwest Research Institute 8500 Culebra Road San Antonio 6, Texas
1	Mr. M. W. Rubesin Vidya Corporation 2626 Hanover Street Palo Alto, California

UNCLASSIFIED